



Search for physics beyond the standard model in final states with a lepton and missing transverse energy in proton-proton collisions at $\sqrt{s} = 8$ TeV

The CMS Collaboration*

Abstract

A search for new physics in proton-proton collisions having final states with an electron or muon and missing transverse energy is presented. The analysis uses data collected in 2012 with the CMS detector, at an LHC center-of-mass energy of 8 TeV, and corresponding to an integrated luminosity of 19.7 fb^{-1} . No significant deviation of the transverse mass distribution of the charged lepton-neutrino system from the standard model prediction is found. Mass exclusion limits of up to 3.28 TeV at 95% confidence level for a W' boson with the same couplings as that of the standard model W boson are determined. Results are also derived in the framework of split universal extra dimensions, and exclusion limits on Kaluza–Klein $W_{\text{KK}}^{(2)}$ states are found. The final state with large missing transverse energy also enables a search for dark matter production with a recoiling W boson, with limits set on the mass and the production cross section of potential candidates. Finally, limits are established for a model including interference between a left-handed W' boson and the standard model W boson, and for a compositeness model.

Published in Physical Review D as doi:10.1103/PhysRevD.91.092005.

1 Introduction

The standard model (SM) of particle physics is a theory of the structure of matter, describing the properties of all known elementary particles and the forces between them. Being studied experimentally for five decades, its predictions have been verified with very high precision. Despite the great success of the SM, beyond the SM (BSM) physics addresses a variety of open issues. To name a few examples: the relationship of the electroweak and gravitational energy scales must be understood and incorporated in the theory; an underlying concept is needed to explain the origin of the observed three fermion families; astrophysical observations indicate the presence of dark matter (DM) not described in the standard model. Many SM extensions predict additional heavy gauge bosons, including models with extended gauge sectors, designed to achieve gauge coupling unification, and theories with extra spatial dimensions. BSM physics can be detected through observation of significant deviations from SM predictions.

The search presented in this paper is sensitive to deviations from the SM prediction for the transverse mass spectrum of events with a charged lepton (electron or muon) and one or more particles that cannot be directly detected (neutrino, dark matter particle) in the final state. Additionally, events are allowed to include an arbitrary number of jets, as they may originate from initial state radiation. Interpretations of the observations are made in the context of various theoretical models: the sequential standard model (SSM) with a W' boson [1], a helicity-non-conserving contact interaction model (HNC-CI) [2], a dark matter (DM) model with a DM particle recoiling against a W boson [3–5], the sequential standard model with a W' boson interfering with the W boson (SSMS, SSMO) [6–8], split universal extra dimensions (split-UED) [9, 10], and a TeV^{-1} model [11–14], the latter two predicting an additional spatial dimension.

Since the discovery of the W boson, experiments have scrutinized the lepton and missing transverse energy channel for evidence of physics beyond the standard model. Neither searches by the Tevatron experiments D0 [15] and CDF [16], nor searches carried out previously at the LHC experiments ATLAS [17–20] and CMS [21–24], have found any indication for such a deviation. The present analysis improves upon the discovery potential of its predecessors. It is based on data from an integrated luminosity of $19.7 \pm 0.5 \text{ fb}^{-1}$ [25] of proton-proton collisions at a center-of mass energy of 8 TeV, recorded in 2012 with the CMS detector [26] at the CERN LHC.

The search for new physics is carried out in the transverse invariant mass distribution. The shape of the distribution is taken into account by using a binned likelihood method. This approach is especially important as the examined theories predict very different signal event distributions. While the SSM W' boson can be discovered at very high transverse mass, the DM and CI models manifest themselves as event excesses at lower values of the transverse mass. A W' boson interfering with the standard model W boson can even lead to a deficit of events in some regions compared to the SM prediction.

This paper is structured as follows. Section 2 describes the experimental setup. The theoretical models are explained in Section 3. A discussion of the event reconstruction and selection criteria in Section 4 is followed by a presentation of the transverse mass distribution of the selected events in Section 5. In Section 6 detailed information about the relevant background processes and their prediction is given. A thorough determination of the uncertainties (Section 7) is essential in order to interpret the results. Limit-setting procedures are explained in Section 8. In Section 9 the limits in terms of the different signal models are derived. A summary of the results is given in Section 10.

2 CMS detector

The central feature of the CMS apparatus is a superconducting solenoid of 6 m internal diameter, providing a magnetic field of 3.8 T. Within the superconducting solenoid volume are a silicon pixel and strip tracker, a lead tungstate crystal electromagnetic calorimeter (ECAL), and a brass/scintillator hadron calorimeter (HCAL), each composed of a barrel and two endcap sections. Muons are measured in gas-ionization detectors embedded in the steel flux-return yoke outside the solenoid. Extensive forward calorimetry complements the coverage provided by the barrel and endcap detectors.

The electromagnetic calorimeter consists of 75 848 lead tungstate crystals which provide coverage in pseudorapidity $|\eta| < 1.479$ in a barrel region (EB) and $1.479 < |\eta| < 3.0$ in two endcap regions (EE).

The ECAL energy resolution for electrons with a transverse energy $E_T \approx 45$ GeV from $Z \rightarrow ee$ decays is better than 2% in the central region of the ECAL barrel ($|\eta| < 0.8$), and is between 2% and 5% elsewhere [27]. For high energies, which are relevant for this analysis, the electron energy resolution slightly improves [28].

Muons are measured in the pseudorapidity range $|\eta| < 2.4$, with detection planes made using three technologies: drift tubes, cathode strip chambers, and resistive plate chambers. Matching muons to tracks measured in the silicon tracker results in a relative transverse momentum resolution in the barrel of about 1% for muons with a transverse momentum p_T of up to about 200 GeV and better than 10% for high momentum muons of $p_T \sim 1$ TeV [29].

A more detailed description of the CMS detector, together with a definition of the coordinate system used and the relevant kinematic variables, can be found in Ref. [26].

3 Physics models and signal simulation

Many models of new physics predict W -boson-like particles decaying with an experimental signature of a charged lepton ℓ and missing transverse energy E_T^{miss} , which may flag the presence of a non-interacting particle. \vec{p}_T^{miss} is defined as $-\sum \vec{p}_T$ of all reconstructed particles with E_T^{miss} being the modulus of \vec{p}_T^{miss} . These additional heavy vector bosons may arise in models with more symmetry groups, extra dimensions, compositeness, or other scenarios. Their presence may be detected as a feature in the observed spectrum of transverse mass, defined as

$$M_T = \sqrt{2p_T^\ell E_T^{\text{miss}} (1 - \cos[\Delta\phi(\ell, \vec{p}_T^{\text{miss}})])}, \quad (1)$$

where $\Delta\phi(\ell, \vec{p}_T^{\text{miss}})$ is the azimuthal opening angle between the directions of the missing transverse energy and that of the charged lepton. The spectrum is expected to be dominated by the W boson background, which has a very small cross section at high M_T . Most new physics models predict high- p_T leptons, which should be identifiable in the low-background region.

This section summarizes the new physics models used for interpretation of the observations, along with model-specific assumptions and details of the generator programs used for production of simulated signal event samples. All generated signal events are processed through a full simulation of the CMS detector based on GEANT4 [30, 31], a trigger emulation, and the event reconstruction chain. An overview of the models considered is given in Table 1. Three representative signal examples (sequential standard model, contact interactions, and dark matter) are used as examples in the distributions throughout the paper. Diagrams of these three signals are shown in Fig. 1. In addition, specific model variations are discussed: the sequential standard

model with W - W' interference (SSMO and SSMS) and two models with one extra dimension and selective particle couplings to this dimension. All limits are given at 95% confidence level (CL) unless stated otherwise.

The analysis is performed in two channels: the $e + E_T^{\text{miss}}$ and the $\mu + E_T^{\text{miss}}$ channel, where the charged lepton is required to be prompt. Final states where the electron or muon originates from, e.g., a τ decay, are not considered as a signal. Therefore, the results can be interpreted for each coupling individually. Only the dark matter model is exempt from that rule. In this model the lepton is produced via a standard model interaction as shown in Fig. 1, and thus events with non-prompt leptons originating from τ decays are also considered.

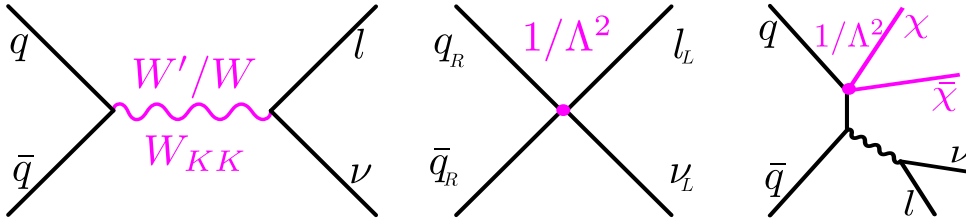


Figure 1: Production and decay of an SSM W' or W_{KK} boson (left); HNC-CI (center); DM single W boson production (right).

3.1 The Sequential Standard Model W' boson

In the SSM, the W' boson, as shown in Fig. 1 (left), is considered to be a heavy analogue of the SM W boson, with similar decay modes and branching fractions. These are modified by the presence of the $t\bar{b}$ decay channel, which opens up for W' boson masses above 180 GeV. Dedicated searches in this channel are described in Refs. [32–37]. This analysis considers W' boson masses of ≥ 300 GeV, yielding a predicted branching fraction (\mathcal{B}) of about 8.5% for each of the leptonic channels studied. Under these assumptions, the width of a 1 TeV W' boson would be about 33 GeV. Decays of the W' boson via WZ are assumed to be suppressed; dedicated searches for these decays can be found in Refs. [38, 39].

The SSM [1] is a benchmark model used as a reference point for experimental W' boson searches for more than two decades. The Tevatron experiments D0 and CDF established mass exclusion limits of around 1.00 TeV [15] and 1.12 TeV [16], respectively. The W' boson searches were among the first analyses to be performed at the LHC, exploiting the large center-of-mass energy. The LHC experiments ATLAS and CMS have more recently raised the W' boson mass exclusion to values around 2.5 TeV [17–19, 21–24].

In accordance with previous analyses [15–19, 21–24], no interference with the SM W boson is considered. The absence of interference can be interpreted as the result of a $V+A$ coupling of the SSM W' boson. The signature of a charged high-momentum lepton and missing transverse energy would be observed in the decays of such a W' boson predicted by left-right symmetric models [40–43]. This particle is typically assumed to have a heavy right-handed neutrino among its decay products [44–46]. However, the mass of the right-handed neutrino is not constrained, and it could be light as long as it does not couple to SM weak bosons. The transverse-mass signature is a Jacobian peak, similar to that of the SM W boson but at much higher masses, as shown by the blue line in Fig. 3 (top left). With increasing W' -boson masses the phase space for production in pp collisions at 8 TeV decreases, because of constraints from the PDFs, leading to a growing fraction produced off-shell at lower masses.

The simulation of data samples in the SSM is performed at leading order (LO) with PYTHIA 6.4.26 [47], using the CTEQ6L1 parton distribution functions (PDF) [48]. A W' boson mass

Table 1: Overview of models considered, with the relevant model parameters. The models are explained in the text with more detail.

Model name	Parameters	Description
Sequential standard model without interference (SSM) [1]	$M_{W'}$	The SSM W' boson does not interfere with the W boson. It has the same coupling strength to fermions as the W boson and its decay width is determined by its mass.
Helicity-non-conserving contact interaction model (HNC-CI) [2]	Λ	A four-fermion contact interaction model. Quarks and leptons are composite objects of fundamental constituents. No interference effects occur in this model.
Dark matter effective theory (DM) [3–5]	M_{χ}, Λ, ζ	A dark matter model with W -boson radiation. Fermionic dark matter particles have a effective coupling to quarks. An SM W boson recoils against the pair of dark matter particles.
Sequential standard model with same sign couplings (SSMS) [6–8]	$M_{W'}$	The SSMS W' boson interferes with the SM W boson and couples in the same way to fermions. This leads to a destructive interference for $M_W < M_T < M_{W'}$ and to a constructive interference for $M_T > M_{W'}$. The coupling strength can vary, resulting in different widths.
Sequential standard model with opposite sign couplings (SSMO)	$M_{W'}$	Similar to SSMS, with the W and W' boson couplings to quarks having the opposite sign. This leads to a constructive interference for $M_W < M_T < M_{W'}$. The coupling strength can vary, resulting in different widths.
Split universal extra dimensions model (split-UED) [9, 10]	μ, R	The tower of $W_{\text{KK}}^{(n)}$ Kaluza–Klein excitations has the same couplings as the W boson. Only if the degree of excitation n is even $W_{\text{KK}}^{(n)}$ boson couples to SM fermions. The LHC is expected to be sensitive only to the second excitation in the tower ($n = 2$). The size of the extra dimension R determines the mass of the $W_{\text{KK}}^{(n)}$ boson. Interference with the SM W boson is not considered.
TeV^{-1} model with a single additional spatial dimension (TeV^{-1}) [11–14]	M_C	SM W bosons propagate into the additional dimension as Kaluza–Klein states. Their coupling constant to fermions is $\sqrt{2}$ times larger than that of the SM W boson. The compactification scale is denoted M_C in this model.

dependent K-factor is used to correct for next-to-next-to-leading order (NNLO) QCD cross sections, calculated using FEWZ [49, 50]. The K-factors vary from 1.363 to 1.140. Table 2 shows the LO and NNLO cross sections for this model. The NNLO corrections decrease with W' -boson masses up to around 2.5 TeV. For higher masses, the K-factor increases and becomes similar to the low-mass values, because of the increased fraction of off-shell production (see Table 2).

3.2 Contact interactions in the helicity-non-conserving model

Another interpretation of an enhancement in the $\ell + E_T^{\text{miss}}$ final state can be made in terms of a specific four-fermion contact interaction (CI), shown schematically in Fig. 1 (middle). The considered model assumes that quarks and leptons are composite objects with fundamental constituents [51], motivated by the observation of mass hierarchies in the fermion sector.

At energies much lower than the binding energy, denoted Λ , the quark and lepton compositeness manifests itself as a four-fermion CI. The CI between two quarks, a neutrino, and a charged lepton is described by the helicity-non-conserving (HNC) model [2]. The corresponding cross section is $\sigma_{\text{CI} \rightarrow \mu\nu} = (\pi\hat{s})/(12\Lambda^4)$, where \hat{s} is the center-of-mass energy of the partons. Typical cross sections for different values of Λ are shown in Table 2. In the HNC model there is no interference of the final state with the SM W boson because of the difference in the chiral structures. The M_T spectrum for CI would yield a non-resonant excess, increasing with M_T relative to the SM expectation, shown in Fig. 3 (top right). Until recently, no limit on the compositeness energy scale had been set in the muon channel in the HNC-CI model. A previous version of this analysis [24] set a limit of 10.5 TeV and updated the previous CDF limit in the electron channel from $\Lambda = 2.81$ TeV [52].

Signal samples for this model were produced with PYTHIA at LO. There are no existing higher-order calculations for this model, and LO cross sections are used.

3.3 Dark matter

One commonly used method to describe direct dark matter production at colliders is the use of an effective field theory (EFT) [3–5]. The matrix element is a four-fermion contact interaction with two quarks in the initial state and two fermionic dark matter particles ($\chi\bar{\chi}$) in the final state. This process would not result in any directly detectable final state objects. The process may be triggered and analyzed through observation of a SM W boson recoiling against the dark matter, as shown in Fig. 1 (right). A search in this leptonic decay mode complements established monojet and monophoton searches [53, 54] and has the advantage of lower SM background, as well as the presence of a lepton to trigger the event. This study of the single-lepton channel follows the strategy outlined in Ref. [55]. Because the p_T sum of non-interacting particles must be balanced by the charged one, we use two-body decay kinematics for the reconstruction of these events.

Under the assumption of a weakly-interacting particle, different couplings are possible. In analogy with the SM weak interaction, the following two couplings are assumed:

$$\begin{aligned} \text{Spin-independent vector coupling:} & \quad \frac{1}{\Lambda^2} \bar{\chi} \gamma^\mu \chi \cdot \lambda_i \bar{q}_i \gamma_\mu q_i \\ \text{Spin-dependent axial-vector coupling:} & \quad \frac{1}{\Lambda^2} \bar{\chi} \gamma^\mu \gamma^5 \chi \cdot \lambda_i \bar{q}_i \gamma_\mu \gamma^5 q_i. \end{aligned}$$

The model parameters are the scale of the effective interaction $\Lambda = M_{\text{messenger}}/\sqrt{g_{\text{DM}}}$, which combines a heavy messenger particle with its coupling constants to dark matter and to quarks g_{DM} . The mass of the dark matter particle is denoted M_χ and is included in the spinors χ and $\bar{\chi}$.

Table 2: Signal production cross sections.

Sequential SM W' boson						
Particle mass	$\sigma_{\text{LO}} \mathcal{B}$ (pb)	K-factor		$\sigma_{\text{NNLO}} \mathcal{B}$ (pb)		
$m_{W'} = 300 \text{ GeV}$	110	1.4		150		
$m_{W'} = 900 \text{ GeV}$	1.5	1.3		2.0		
$m_{W'} = 2000 \text{ GeV}$	0.021	1.2		0.026		
$m_{W'} = 3000 \text{ GeV}$	0.0013	1.2		0.0015		
$m_{W'} = 4000 \text{ GeV}$	0.00025	1.3		0.00033		
Contact interactions in the helicity-non-conserving model						
Λ (TeV)	3	4	7	9		
$\sigma_{\text{LO}} \times B$ (pb)	0.54	0.17	0.018	0.0067		
Dark matter						
interference parameter ζ	1	0	-1	1	0	-1
Particle mass	$\sigma_{\text{LO}} \mathcal{B}$ (pb)			χ -proton cross section (pb)		
Spin-independent $\Lambda = 200 \text{ GeV}$						
$M_\chi = 3 \text{ GeV}$	3.1	7.4	26.5	3.6	1.6	0.4
$M_\chi = 100 \text{ GeV}$	2.9	7.1	25.2	6.0	2.7	0.7
$M_\chi = 300 \text{ GeV}$	1.9	4.8	17.2	6.1	2.7	0.7
$M_\chi = 500 \text{ GeV}$	1.0	2.5	9.1	6.1	2.7	0.7
$M_\chi = 1000 \text{ GeV}$	0.1	0.3	0.9	6.1	2.7	0.7
Spin-dependent $\Lambda = 200 \text{ GeV}$						
$M_\chi = 3 \text{ GeV}$	3.1	7.4	26.5	0.2	0.8	1.9
$M_\chi = 100 \text{ GeV}$	2.5	6.4	22.8	0.3	1.4	3.2
$M_\chi = 300 \text{ GeV}$	1.2	3.1	11.1	0.4	1.4	3.3
$M_\chi = 500 \text{ GeV}$	0.5	1.2	4.3	0.4	1.4	3.3
$M_\chi = 1000 \text{ GeV}$	0.03	0.1	0.2	0.4	1.4	3.3
Models with interference of W and W' bosons (W boson LO cross section subtracted)						
Particle mass	SSMS $\sigma_{\text{LO}} \mathcal{B}$ (pb)			SSMO $\sigma_{\text{LO}} \mathcal{B}$ (pb)		
$m_{W'} = 300 \text{ GeV}$	33 ± 59			90 ± 81		
$m_{W'} = 500 \text{ GeV}$	11 ± 58			21 ± 57		
$m_{W'} = 1000 \text{ GeV}$	0.12 ± 0.85			1.562 ± 0.099		
$m_{W'} = 2000 \text{ GeV}$	-0.030 ± 0.040			0.0460 ± 0.0079		
$m_{W'} = 3000 \text{ GeV}$	-0.0064 ± 0.0013			0.0125 ± 0.0018		
split-UED $W_{\text{KK}}^{(2)}$ boson						
Particle mass	$\mu = 0.05 \text{ TeV}$			$\mu = 10 \text{ TeV}$		
	$\sigma_{\text{LO}} \mathcal{B}$ (pb)	$\sigma_{\text{NNLO}} \mathcal{B}$ (pb)		$\sigma_{\text{LO}} \mathcal{B}$ (pb)	$\sigma_{\text{NNLO}} \mathcal{B}$ (pb)	
$m_{W_{\text{KK}}^{(2)}} = 300 \text{ GeV}$	42	56		250	340	
$m_{W_{\text{KK}}^{(2)}} = 500 \text{ GeV}$	2.3	3.1		37	51	
$m_{W_{\text{KK}}^{(2)}} = 1000 \text{ GeV}$	0.030	0.040		2.0	2.7	
$m_{W_{\text{KK}}^{(2)}} = 2000 \text{ GeV}$	0.00013	0.00016		0.050	0.061	
$m_{W_{\text{KK}}^{(2)}} = 3000 \text{ GeV}$	0.0000014	0.0000016		0.0042	0.0048	
TeV^{-1} model (W boson LO cross section subtracted)						
Particle mass	$\sigma_{\text{LO}} \mathcal{B}$ (pb)					
$M_C = 2000 \text{ GeV}$	-0.966 ± 0.025					
$M_C = 2600 \text{ GeV}$	-0.079 ± 0.014					

The parameter λ_i introduces a relative coupling strength, which in general could be different for each quark flavor.

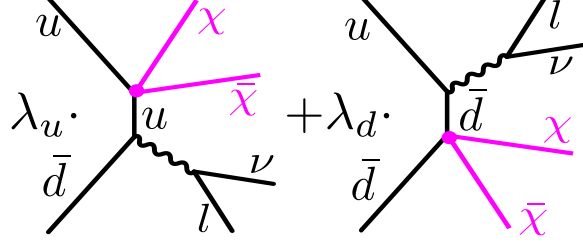


Figure 2: Feynman diagrams for dark matter interference, shown as an example with an up and a down quark. The same initial and final state can have different particles coupling to the dark matter particles.

Dark matter can couple to either up- or down-type quarks with the same initial and final state, as shown in Fig. 2. Given that the couplings to up- or down-type quarks yield similar behavior, the parameter $\zeta = \lambda_u \lambda_d$ is most important for the phenomenology. Following Ref. [55], we consider three scenarios with $|\lambda_i|=1$ or 0. A value of $\zeta = \pm 1$ maximizes the effects of interference. A choice of $\zeta = 0$ can be assumed in two different ways, suppressing either the coupling to up- or to down-type quarks. Both cases are shown in Fig. 3 (middle left). The difference between the two cases is small, therefore in the following we only consider the case with suppressed couplings to down-type quarks ($\lambda_d = 0$) and denote it as $\zeta = 0$. The choice of the interference parameter changes the total cross section and the shape of the M_T spectrum, as shown in Fig. 3 (middle left) for $\Lambda = 600$ GeV, $M_\chi = 10$ GeV.

In searches at proton-proton colliders, the difference between vector and axial-vector coupling is less important than in direct DM-nucleon interaction experiments, as can be seen from Table 2. This is due to the large influence of the spin on the interaction at low Q^2 (of the order of 1 to 100 keV [56]), which is relevant for direct detection experiments, where coherent scattering at the nucleus is only possible for spin-independent (vector) couplings, but not for the spin-dependent (axial-vector) couplings. At the LHC, half of the initial quarks originate from the quark-gluon sea, and all spin configurations and light-quark flavors are available for production. For low M_χ , no difference is observed between vector and axial-vector couplings, as shown in Fig. 3 (middle left) for $M_\chi = 10$ GeV. For masses above 100 GeV, axial-vector cross sections are lower than the vector cross sections, without a significant shape difference.

The validity of this effective-theory model is limited. For $\Lambda > M_\chi/2\pi$ the coupling is perturbative. A more stringent criterion is $g_{\text{DM}} = 1$, which constrains the model to $\Lambda > 2M_\chi$.

Simulated signal samples are produced with MADGRAPH 5.1.5 [57] matched to PYTHIA for showering and hadronization. The search is inclusive in terms of jet multiplicity, and no constraints on the number of jets are applied. The samples are simulated for $\zeta = +1$ and are rescaled on an event-by-event basis for $\zeta = 0$ and -1 .

3.4 Interference of W and W' bosons with variable coupling strength

If the W' boson interacts with left-handed particles and right-handed antiparticles (V-A coupling), interference with the W boson is expected [6–8]. The lowest-order effective Lagrangian for the interaction of two fermions and such a W' boson is

$$\mathcal{L} = \frac{V^{ij}}{2\sqrt{2}} g_{W'}^{ij} \bar{f}^i \gamma^\mu (1 - \gamma^5) W'_\mu f^j + \text{h.c.}, \quad (2)$$

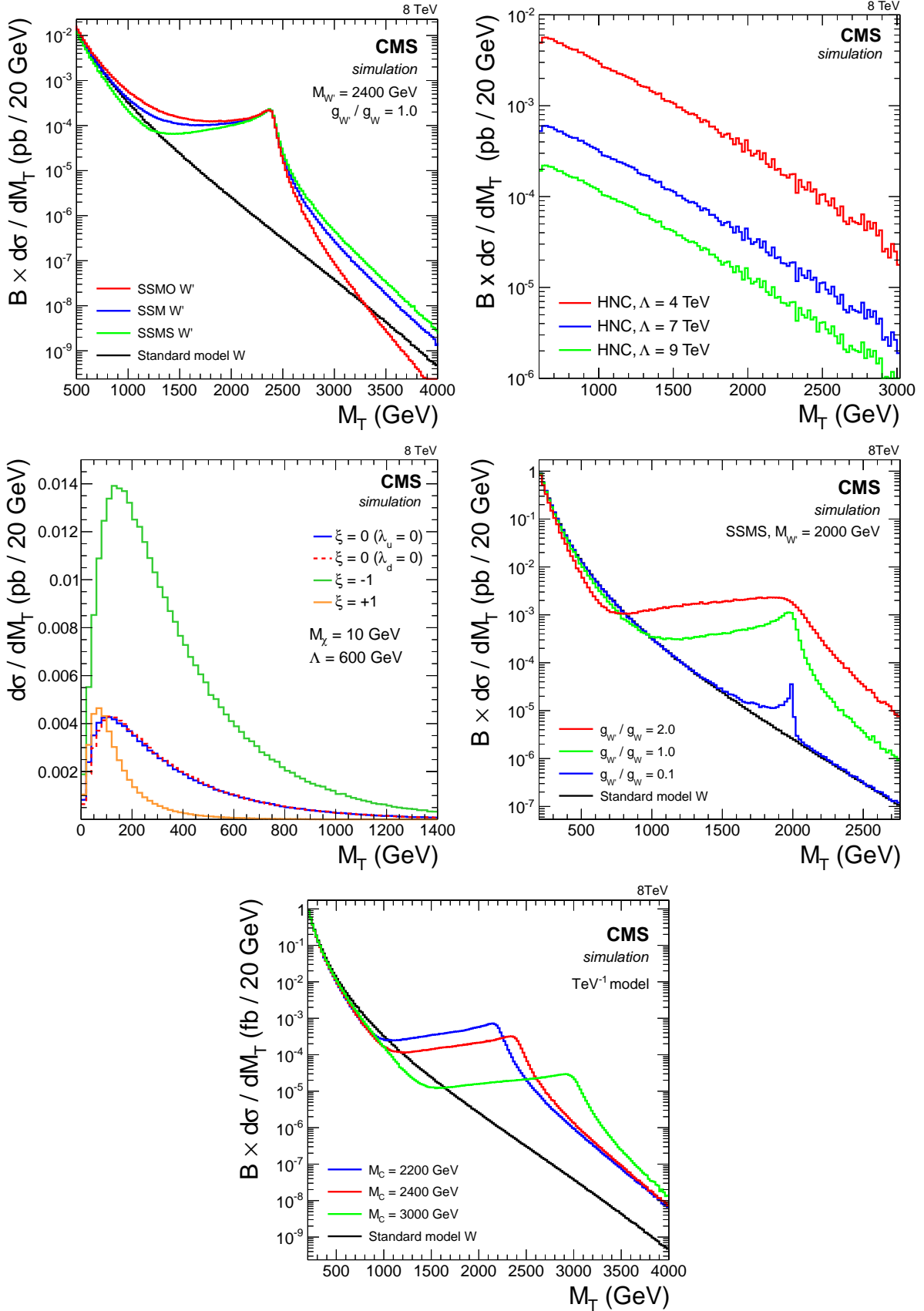


Figure 3: Signal shapes at generator level: SSM model compared to the SSMS and SSMO models for $g_{W'}/g_W = 1$ (top left); HNC-CI model for various values of Λ (top right); DM for various values of ξ (middle left); W' with W boson interference and a varying coupling strength $g_{W'}/g_W$ in the same sign scenario (middle right); and TeV^{-1} model (bottom).

where h.c. is the hermitian conjugate, V_{ij} is the CKM matrix element for quarks and unity for leptons, and $g_{W'}$ is the coupling constant. The nature of the interference effects depends on the ratio of the coupling $g_{W'}$ to the SM weak coupling constant $g_W = e/\sin\theta_W$. Two different scenarios are considered: the same sign scenario (SSMS) with $g_{W'}^{\ell\nu}g_{W'}^{qq'} > 0$, and the opposite sign scenario (SSMO) with $g_{W'}^{\ell\nu}g_{W'}^{qq'} < 0$. The absolute value of the coupling $g_{W'}$ is considered the same for quarks and leptons.

For the SSMS, the differential cross section for $W + W'$ boson production can be smaller than the SM W boson cross section, reflecting the effect of destructive interference. This effect is shown by the green curve in Fig. 3 (top left) and is discussed in Ref. [6]. In the SSMO, the cross sections exceed the SSM cross sections because of constructive interference, shown by the red curve in the same figure.

The coupling strength $g_{W'}$ affects both the total cross section and the width of the Jacobian peak. It also influences the impact of the interference effects on the M_T spectrum. Assuming $g_{W'} = g_W$ the Jacobian peak partial widths of a W' boson decaying to leptons can be seen in Fig. 3 (top left). For a larger coupling, the width increases, as shown in Fig. 3 (middle right). This behavior is taken into account when deriving mass limits as a function of the coupling strength. A similar strategy was used in previous $W' \rightarrow tb$ analysis [15, 33].

The contributions of the W and W' bosons to the overall cross section must be simulated simultaneously, as the final scattering amplitude is the sum of these two terms squared. An M_T requirement is used at event generation to reduce the W boson contribution resulting from the large W boson production cross section, which is several orders of magnitude larger than that for the W' boson production: $\sigma_{\text{LO}}(W \rightarrow \ell\nu)$ falls from 9600 pb to 1.5 fb when the requirement $M_T > 500$ GeV is imposed.

To provide an impression about the influence of the W' boson on the total cross section, effective cross sections are provided in Table 2 for the SSMS and SSMO models. They are derived from simulations of $W + W'$ boson production with interference, with subsequent subtraction of the W boson background. For each mass point, an individual M_T cut-off is chosen and applied to both the W boson sample and the $W + W'$ sample before subtraction. This lowers the W boson contribution and therefore reduces the large uncertainty induced when subtracting two large and similar numbers. The cut-off is selected at the M_T value where the two distributions are compatible within their statistical uncertainties. For example, the cut-off for the W' boson of 2 TeV in mass has been chosen to be 250 GeV. It is then varied up and down by 40 GeV to represent the interval in which the two distributions approach each other and the procedure is repeated. The difference of the varied subtractions is provided as uncertainty in Table 2. The resulting effective W' cross section can be compatible with 0 or even less in case of destructive interference. These effective cross sections are meant to provide additional information for the reader and not used in the analysis, which is based on the combined $W + W'$ boson production cross section.

A model of a W' boson with an SM-like left-handed coupling has been implemented within the MADGRAPH 4.5.1 event generator [58]. This model includes spin correlations as well as finite-width effects. For each W' -boson mass hypothesis, a sample with $g_{W'} = g_W$ is processed by PYTHIA with the Z2* [59] tune, in order to simulate showering and hadronization. This sample is then reweighted using MADGRAPH in order to simulate the M_T distribution for different values of the W' boson couplings. Both generators simulate at LO. The CTEQ6L1 PDF [48] is employed.

To correct for higher-order effects in W boson production, the difference between the next-

to-leading order (NLO) and LO event yields are taken into account in the transverse mass distribution. For the W' boson contribution, the LO cross sections have been used.

3.5 Split-UED model

The leptonic final states under study may also be interpreted in the framework of universal extra dimensions with fermions propagating in the bulk, known as split-UED [9, 10]. This is a model based on an extended space-time with an additional compact fifth dimension of radius R . In this model all SM particles have corresponding Kaluza–Klein (KK) partners, for instance $W_{\text{KK}}^{(n)}$, where the superscript denotes the n th KK excitation mode. Only KK-even modes of $W_{\text{KK}}^{(n)}$ couple to SM fermions, owing to KK-parity conservation. Modes with $n \geq 4$ are not expected to be accessible under present LHC conditions, hence the only mode considered is $n = 2$. Interference with the SM is not considered in this model. Under this assumption, the decay to leptons is kinematically identical to the SSM W' boson decay, and the observed limits obtained from the $W' \rightarrow e\nu$ and $W' \rightarrow \mu\nu$ searches can be reinterpreted directly in terms of the $W_{\text{KK}}^{(n)}$ -boson mass, taking into account the difference in widths in the simulation. The LO and NNLO production cross sections for a $W_{\text{KK}}^{(2)}$ boson are shown in Table 2.

The UED model is parameterized by the quantities R and μ , which are the radius of the extra dimension and the bulk mass parameter of the fermion field in five dimensions. In the split-UED model the parameter μ is assumed to be non-zero, following Refs. [9, 10].

The mass of the $W_{\text{KK}}^{(n)}$ is determined by $M_{W_{\text{KK}}^{(n)}} = \sqrt{M_W^2 + (n/R)^2}$, i.e. a larger radius corresponds to smaller KK masses. The mass of KK fermions depends on the bulk mass parameter μ . The cross section of the $W_{\text{KK}}^{(n)}$ production times the branching fraction to standard model fermions goes to zero as μ goes to zero.

3.6 Model with a TeV^{-1} extra dimension

Another extra dimensions model, the TeV^{-1} model, has been proposed [11–14], in which only the fermions are confined to ordinary three-dimensional space, with the SM gauge bosons and the Higgs field propagating in compactified extra dimensions. Under the assumption of a single extra dimension, the model is specified by one parameter $R = 1/M_C$, the size of the compactified dimension, with M_C being the corresponding compactification scale. The W bosons propagating in the compactified dimension are equivalent to the KK states $W_{\text{KK}}^{(n)}$ with masses $M_n = \sqrt{M_0^2 + (n/R)^2}$, where M_0 is the mass of the SM W boson. The coupling constant of the KK states (for $n > 0$) to fermions is $\sqrt{2}$ times larger than that of the SM W boson.

The signal is similar in shape to an SSM W' boson with destructive interference, as seen in Fig. 3 (bottom). This results in effective cross sections of -0.966 ± 0.025 fb for the $M_C = 2.0$ TeV case and -0.079 ± 0.014 fb for the $M_C = 2.6$ TeV case with respect to the W boson.

Given the absence of higher-order calculations, the samples are generated at LO with MADGRAPH 5.1.3.22 using the CTEQ6L1 parton distribution functions. The cross sections with the W boson cross section subtracted are summarized in Table 2.

4 Object identification and event selection

The models described in the previous section provide an event signature of a single high- p_T lepton (electron or muon) and one or more particles that cannot be detected directly (neutrino,

dark matter particle), and so give rise to experimentally observed E_T^{miss} . This quantity is measured using a particle-flow technique [60–62], an algorithm that combines measurements from all components of the CMS detector in order to produce particle candidates. The modulus of the vector p_T sum of these candidates defines E_T^{miss} , which is corrected for the jet energy calibration [63, 64]. At high M_T , the calculation of E_T^{miss} is dominated by the high- p_T lepton in the event.

Candidate events with at least one high- p_T lepton are selected using single-muon (with $p_T > 40$ GeV) and single-electron (with $E_T > 80$ GeV) triggers and loose electron identification criteria. The relatively high electron trigger threshold is required in order to suppress non-prompt electrons and jets. In the muon channel, the offline reconstructed p_T must be greater than 45 GeV, where the trigger is already fully efficient. This relatively low p_T requirement does not impair the search in the high- M_T region, while preserving an adequate number of events in the low- and medium- M_T control regions. The requirement of $E_T > 100$ GeV in the electron channel ensures a constant and high trigger efficiency. The trigger efficiency for single electrons has been determined with “tag-and-probe” methods [65] to be 99.1 (97.6)% for the barrel (endcap) ECAL, with a data-to-simulation scale factor of nearly one. The single-muon trigger efficiency varies from 94% in the barrel to 82% in the endcap regions, with data-to-simulation scale factors of 0.98–0.96 [66].

Electrons are reconstructed as ECAL clusters that are matched to a tracker track and their identification has been optimized for high- p_T [28]. They have to be sufficiently isolated, have an electron-like shape and be within the acceptance region of the barrel ($|\eta| < 1.442$) or the endcaps ($1.56 < |\eta| < 2.5$). This acceptance region avoids the gap between barrel and endcap, where the misidentification probability is the highest. Electron isolation in the tracker is ensured by requiring the p_T sum of all tracks that are in close proximity to the track of the electron candidate and originate from the same primary vertex, to be less than 5 GeV. Here, only tracks that are within a cone of $\Delta R = 0.3$ around the electron candidate’s track are considered. The primary vertex is defined as the vertex with the highest $\sum p_T^2$ in the event, where the sum extends over the charged tracks associated with the vertex. In the calorimeters, the E_T sum of energy deposits around the electron candidate is used as a measure of isolation. It is corrected for the mean energy contribution from additional proton proton collisions during the same bunch crossing (pileup). As in the tracker isolation calculation, contributions within a $\Delta R < 0.3$ cone around the electron candidate are considered. To obtain sufficiently isolated electrons, this calorimeter isolation is required to be below a threshold of around 3% of the electron’s E_T . Additionally, the energy deposits in the hadron calorimeter within a cone of $\Delta R = 0.15$ around the electron’s direction must be less than 5% of the electron’s energy deposit in the ECAL. In order to differentiate between electrons and photons, properties of the track matched to the calorimeter measurement must be consistent with those of a prompt electron. Specifically, there must be ≤ 1 hit missing in the innermost tracker layers, and the transverse distance to the primary vertex must be < 0.02 cm (barrel) or < 0.05 cm (endcap). To reduce the Drell–Yan background, events with additional electrons of $E_T > 35$ GeV are rejected.

The reconstruction of muons is optimized for high p_T . Information from the inner tracker and the outer muon system are used together. Each muon is required to have at least one hit in the pixel detector, at least six tracker layer hits, and segments in two or more muon detector layers. Since segments are typically found in consecutive layers separated by thick layers of steel, the latter requirement significantly reduces the amount of hadronic punch-through [29]. To reduce background from cosmic ray muons, each muon is required to have a transverse impact parameter $|d_0|$ of less than 0.02 cm and to have a longitudinal distance parameter $|d_z|$ of the tracker track of less than 0.5 cm. Both parameters are defined with respect to the primary vertex.

In order to suppress muons with mismeasured p_T , an additional requirement $\sigma_{p_T}/p_T < 0.3$ is applied, where σ_{p_T} is the uncertainty from the track reconstruction. To match the trigger acceptance the muon must have $|\eta| < 2.1$. Muon isolation requires that the scalar p_T sum of all tracks originating from the interaction vertex within a $\Delta R = \sqrt{(\Delta\phi)^2 + (\Delta\eta)^2} < 0.3$ cone around its direction, excluding the muon itself, is less than 10% of the muon's p_T . To further reduce the Drell–Yan and cosmic ray backgrounds, the event must not have a second muon with $p_T > 25$ GeV.

The reconstruction efficiencies for both electrons and muons are measured using same-flavor dilepton events, up to the highest accessible p_T . Data and simulation agree within statistical uncertainties for these high-energy events. For higher p_T , the flat efficiency is extrapolated and assigned an associated systematic uncertainty, as described in Section 7.

In order to identify any differences in selection efficiency for observed and simulated data, efficiencies for both are determined using the “tag-and-probe” method. The total efficiency in each case includes contributions from the trigger, lepton identification, and isolation criteria. The ratio of data to simulation efficiencies, denoted as the scaling factor (SF), is determined to be 0.975 ± 0.023 (0.970 ± 0.042) for barrel (endcap) in the electron channel. For the muon channel, the SFs are 0.967 ± 0.026 for $|\eta| < 0.9$ (barrel), 0.948 ± 0.026 for $0.9 < |\eta| < 1.2$ (barrel-endcap interface), and 0.979 ± 0.026 for $1.2 < |\eta| < 2.1$ (forward region) [66].

In the models considered, the lepton and \vec{p}_T^{miss} are expected to be nearly back-to-back in the transverse plane, and balanced in transverse energy. This is illustrated in Fig. 4 for the muon channel for three example signals (SSM, HNC-CI, and DM) with an M_T threshold of 220 GeV. To incorporate these characteristics in the analysis, additional kinematic criteria select events based on the ratio of the lepton p_T to E_T^{miss} , requiring $0.4 < p_T/E_T^{\text{miss}} < 1.5$, and on the angular difference between the lepton and \vec{p}_T^{miss} , with $\Delta\phi(\ell, \vec{p}_T^{\text{miss}}) > 2.5 \approx 0.8\pi$.

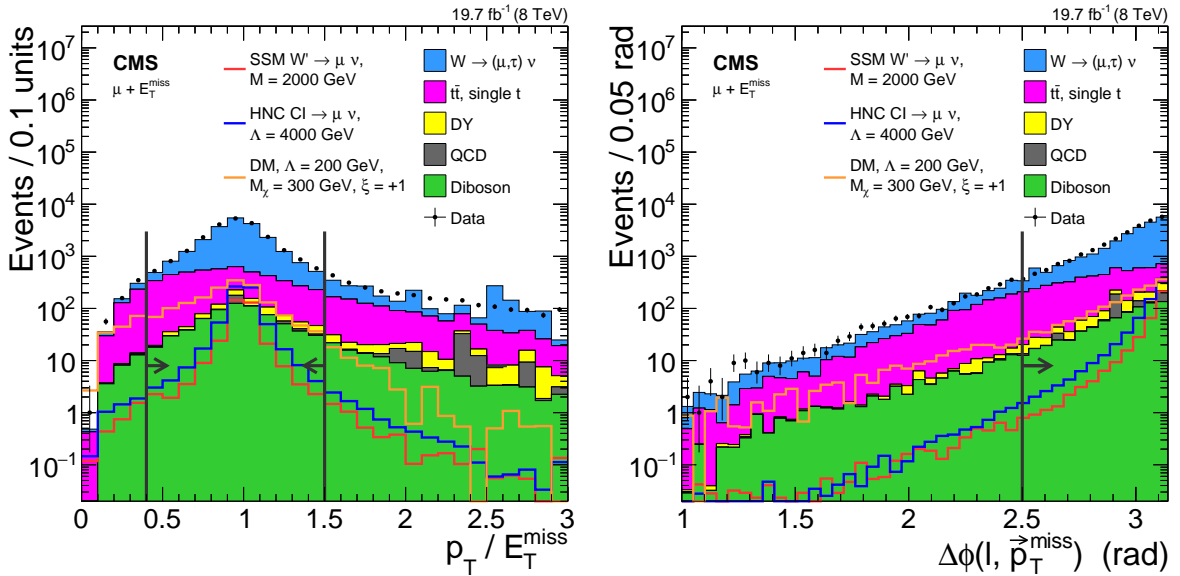


Figure 4: The distribution in p_T/E_T^{miss} (left) and $\Delta\phi(\ell, \vec{p}_T^{\text{miss}})$ (right), for data, background, and some signals in the muon channel with an M_T threshold of 220 GeV. The simulated background labeled as ‘diboson’ includes WW , ZZ and WZ contributions, while ‘DY’ denotes the Drell–Yan process.

Signal efficiencies are model-dependent, determined by the signal shape in the distribution of M_T . For simulated events passing all the selection criteria, the average signal efficiencies for a

given parameter are summarized in Table 3.

Table 3: Signal efficiencies for the various models.

Model	Parameter	Electron channel	Muon channel
SSM W'	$M_{W'} = 0.5 \text{ TeV}$	$62 \pm 3\%$	$64 \pm 3\%$
SSM W'	$M_{W'} = 1.5 \text{ TeV}$	$74 \pm 6\%$	$71 \pm 7\%$
SSM W'	$M_{W'} = 4 \text{ TeV}$	$50 \pm 5\%$	$55 \pm 4\%$
HNC-CI	Λ independent	$80 \pm 6\%$	$80 \pm 6\%$
DM	$\zeta = -1$	$42 \pm 4\%$	$42 \pm 4\%$
DM	$\zeta = 0$	$39 \pm 4\%$	$39 \pm 4\%$
DM	$\zeta = +1$	$12 \pm 2\%$	$13 \pm 2\%$

The SSM W' has maximal signal efficiency at the mass of 1.5 TeV, decreasing gradually for larger and smaller masses. The uncertainties quoted in Table 3 are explained in Section 7. The geometrical acceptance is roughly 90% for both electron and muon channels. For the higher W' -boson masses up to 4 TeV the signal efficiencies slowly decrease to 50%, because of an increasing fraction of off-shell W' bosons.

For the HNC-CI model, the signal efficiency is independent of the interaction scale Λ and has been determined from simulation to be 80% with 6% uncertainty for both the $e + E_{\text{T}}^{\text{miss}}$ signal and the $\mu + E_{\text{T}}^{\text{miss}}$ signals.

For the DM models the signal efficiency depends on the steepness of the M_{T} distribution and the total cross section, both of which are sensitive to the interference parameter ζ . For $\zeta = +1$, the spectrum falls more rapidly, and the search region corresponds to the low-to-medium part of the M_{T} spectrum, resulting in a rather low signal efficiency of $(13 \pm 2)\%$. For the other two interference cases, $\zeta = 0$ and -1 , the spectrum extends to very high M_{T} , where the expected background is negligible and the electron and muon channel signal efficiencies are as high as $(39 \pm 4)\%$ for $\zeta = 0$ and $(42 \pm 4)\%$ for $\zeta = -1$. As expected, no difference in efficiency is observed between the vector and the axial-vector couplings.

5 Distribution in M_{T}

The observed M_{T} distributions for the analyzed data sets are shown in Fig. 5 for the electron and muon channels. Included in the same figure are the predicted M_{T} distributions for the accepted SM events, separated into contributions from each background process, along with example signal distributions for DM, SSM W' , and HNC-CI models. For both channels, a variable binning commensurate with the energy-dependent M_{T} -resolution is used. The expected systematic uncertainty in the M_{T} distribution is also shown.

The deviation of the data from the standard model prediction is shown in Fig. 6. No significant deviation from the predicted background is observed in the M_{T} spectrum. The highest transverse mass events observed have $M_{\text{T}} = 2.3 \text{ TeV}$ in the electron channel and $M_{\text{T}} = 2.1 \text{ TeV}$ in the muon channel. Both events have a well-reconstructed high- p_{T} lepton and very little hadronic activity.

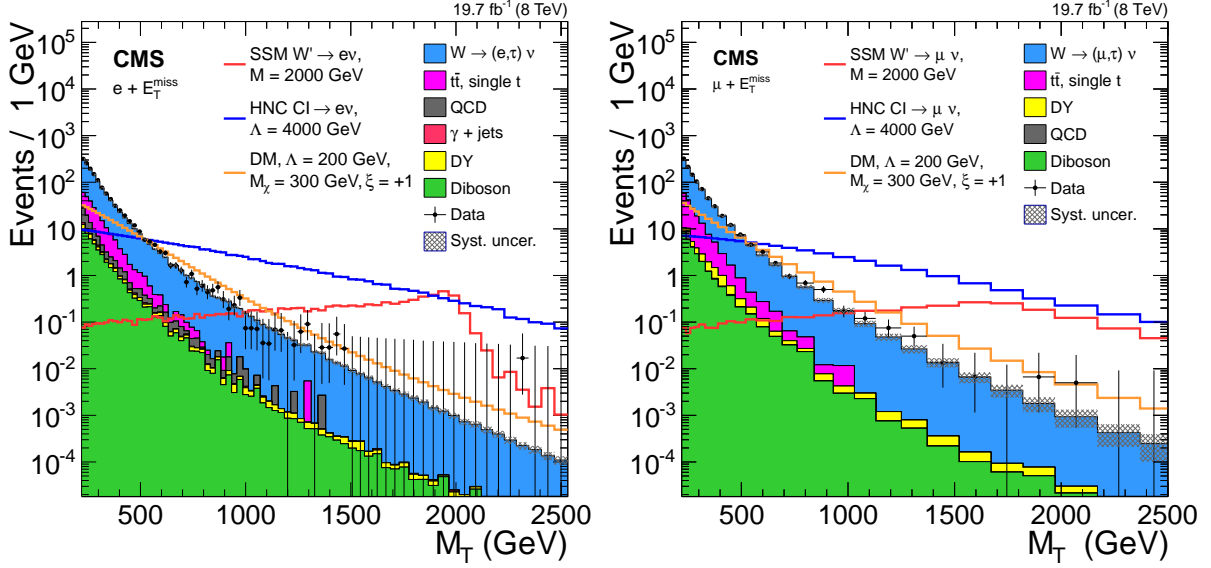


Figure 5: Observed M_T distributions for the electron (left) and muon (right) channels. The horizontal bars on the data points indicate the widths of the bins. The asymmetric error bars indicate the central confidence intervals for Poisson-distributed data and are obtained from the Neyman construction as described in Ref. [67].

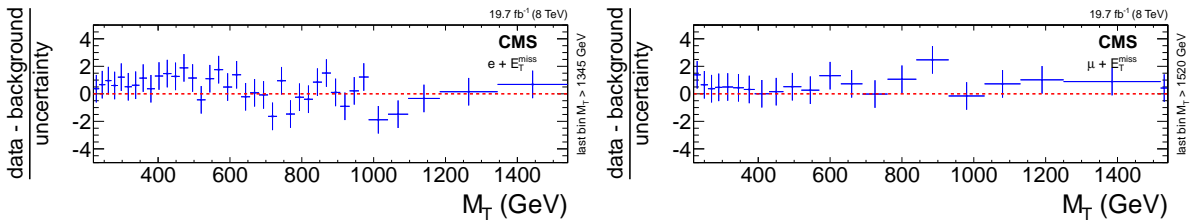


Figure 6: Deviation of the number of observed events from the expectation, as shown in Fig. 5, in units of standard deviations, binned in M_T for the electron (left) and muon (right) channels. Both the systematic and statistical uncertainties are included. The horizontal bars on the data points indicate the widths of the bins, which are chosen as in Fig 5 with the extension to include always 5 background events in a bin.

6 Background

6.1 Sources of background

The primary source of background for all signals is the presence of off-peak, high-transverse-mass tails of the SM $W \rightarrow \ell\nu$ decays. Other important backgrounds arise from QCD multijet, $t\bar{t}$, and Drell–Yan events. Contributions from dibosons (WW , WZ , ZZ) decaying to e , μ , or τ -leptons are also considered. The following background sources are considered in this analysis. They are listed in the order of Fig. 5, where their distribution in M_T can be seen.

1. A $W \rightarrow \ell\nu$ with $\ell = e, \mu$ sample is simulated at LO with PYTHIA. To ensure a good description of the considered phase space, two samples with lepton p_T ranges 100–500 GeV and ≥ 500 GeV, respectively, are used. A transverse-mass-dependent K-factor is calculated, including NLO QCD and electroweak corrections (see Section 6.3).
2. A $W \rightarrow \tau\nu$ sample, where the τ -lepton decays to an electron or a muon and the two corresponding neutrinos, is generated with PYTHIA using the same K-factors as above. Electrons and muons from these decays have a small impact parameter with respect to the primary vertex and are not separable from prompt leptons. In addition, the p_T/E_T^{miss} ratio is approximately one, despite the presence of three neutrinos in the event, since the vector sum of the neutrinos' p_T balances the charged lepton p_T for small W boson p_T . These features prevent an efficient rejection of $W \rightarrow \tau\nu$ events, which therefore contribute to the background, albeit at low M_T (see Fig. 7) and with little contribution in the high- M_T region.
3. Top-quark pair and single top-quark production are other sources of high- p_T leptons and E_T^{miss} , and these are generated with MC@NLO [68, 69] in combination with HERWIG [70], and POWHEG [71–74] in combination with PYTHIA, respectively. A newly calculated NNLO cross section [75] is used to rescale the NLO predictions. These events are largely rejected by the requirement of two-body decay kinematics (see Section 4) but can extend into high M_T as seen in Fig. 5.
4. Multijet background (QCD), enriched in electrons/photons and muons, is generated with PYTHIA. Although this process has by far the largest cross section, it is efficiently rejected by the isolation requirements imposed to select the lepton candidates as well as the requirement on the ratio of p_T/E_T^{miss} (see Section 4). Despite the large suppression of these events, the misidentification of jets as leptons (especially as electrons) still occurs. The contribution of QCD multijet events to the electron channel is derived from data as explained in Section 6.4.
5. Drell–Yan production of dileptons ($\ell = e, \mu$) constitutes a background when one lepton escapes detection. The samples are generated with POWHEG [76]. Contributions from Drell–Yan production of $\tau\bar{\tau}$ are simulated using PYTHIA, applying a uniform QCD K-factor of 1.26 (calculated with FEWZ [49, 50]).
6. Contributions from dibosons (WW , WZ , ZZ) decaying to a state with at least one lepton, are generated with PYTHIA and scaled to NLO cross sections.
7. In the electron channel, a γ +jet event sample, generated with PYTHIA, is used to estimate the effects of photons misidentified as electrons.

Background selection efficiencies for $M_T > 220$ GeV are summarized in Table 4. The total background predictions, listed in Table 5, are comparable in the electron and muon channels.

Resolution effects, reconstruction efficiencies, and statistical fluctuations are taken into account. Systematic uncertainties are discussed in Section 7.

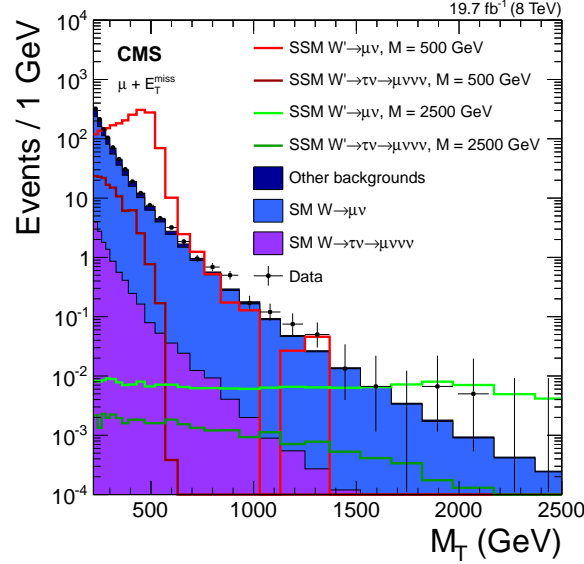


Figure 7: Contributions from W and W' bosons decaying to $\tau\nu \rightarrow \mu\nu\nu\nu$ compared to the prompt $\mu\nu$ decay channel. Also shown are the contributions from the other backgrounds and the number of data events. The horizontal bars on the data points indicate the widths of the bins.

Table 4: Background processes and their number of events N_{events} and selection efficiencies after the full selection and the requirement $M_T > 220$ GeV.

Process	e channel		μ channel	
	N_{events}	selection efficiency	N_{events}	selection efficiency
$W \rightarrow \ell\nu$ with $\ell = e, \mu$	18390 ± 170	$(745.8 \pm 7.0) \times 10^{-7}$	17261 ± 151	$(697.5 \pm 6.1) \times 10^{-7}$
$W \rightarrow \tau\nu, \tau \rightarrow (e, \mu)\nu\nu$	491 ± 74	$(19.8 \pm 3.0) \times 10^{-7}$	281.3 ± 3.4	$(113.7 \pm 1.7) \times 10^{-8}$
Top-quark pair and single top-quark	2831 ± 28	$(398.4 \pm 3.9) \times 10^{-6}$	3132 ± 30	$(486.8 \pm 4.6) \times 10^{-6}$
Diboson	783.8 ± 8.3	$(376.5 \pm 4.0) \times 10^{-6}$	629.6 ± 7.7	$(325.8 \pm 4.0) \times 10^{-6}$
Multijet (QCD)	705 ± 19	data driven	16.5 ± 7.3	$(11.1 \pm 4.9) \times 10^{-12}$
$DY \rightarrow \ell\ell$ with $\ell = e, \mu, \tau$	159 ± 19	$(20.8 \pm 2.5) \times 10^{-7}$	216.1 ± 5.9	$(280.8 \pm 7.6) \times 10^{-8}$
γ +jet	56.7 ± 8.4	$(31.7 \pm 4.7) \times 10^{-7}$	—	—

All simulated event samples are normalized to the integrated luminosity of the recorded data, using calculated NNLO cross sections. The only exceptions are the diboson and QCD samples, for which the NLO and LO cross sections are used, respectively. The simulation of pileup is included in all event samples by superimposing minimum bias interactions onto all simulated events. For the data set used, the average number of interactions per bunch-crossing is 21.

6.2 Prediction of the expected background

Searching for deviations from the steeply falling W -boson M_T spectrum requires an accurate background estimate at very high transverse masses. Several methods are used to evaluate the expected background in the signal region, based either on control samples in data or on a fully simulation-based approach.

For the majority of background sources, the estimate is determined from simulation, based on samples with large event counts at high M_T . However, to avoid bin-to-bin statistical fluctua-

tions that may still occur at very high M_T , the total background prediction is parameterized with the empirical function given in Eq. (3).

$$f(M_T) = e^{a+bM_T+cM_T^2}M_T^d, \quad (3)$$

where a , b , c , and d are the fit parameters. This function was found to provide a good description of the steeply falling SM background up to high M_T . Based on this parameterization, the expected number of SM background events for all transverse mass bins can be predicted, as shown for three typical thresholds M_T^{\min} in Table 5. Contributions from SM processes drop quickly with increasing M_T , leading to an expected yield of less than 0.5 events in each channel, for $M_T > 2$ TeV.

Table 5: Event yields observed in data, and expected from background and signal, for different transverse mass thresholds. The quoted uncertainties are the combined uncertainties assuming a log-normal distribution, not including a 2.6% integrated luminosity uncertainty [25].

		$M_T > 1.0$ TeV	$M_T > 1.5$ TeV	$M_T > 2.0$ TeV
Electron channel				
Data		24	1	1
SM Background		$26.0^{+2.5}_{-2.5}$	$2.02^{+0.26}_{-0.25}$	$0.207^{+0.036}_{-0.033}$
W'	$M_{W'} = 2.5$ TeV	$50.5^{+7.5}_{-7.5}$	$38.8^{+6.1}_{-6.1}$	$24.0^{+3.9}_{-3.9}$
	$M_{W'} = 3$ TeV	$10.3^{+2.1}_{-2.1}$	$7.8^{+1.9}_{-1.9}$	$5.8^{+1.5}_{-1.5}$
HNC-CI	$\Lambda = 4$ TeV	1120^{+110}_{-110}	368^{+47}_{-47}	105^{+19}_{-19}
	$\Lambda = 9$ TeV	$43.4^{+4.3}_{-4.3}$	$14.3^{+1.8}_{-1.8}$	$4.08^{+0.75}_{-0.75}$
DM vector-coupling, $M_\chi = 50$ GeV, $\Lambda = 300$	$\zeta = +1$	$0.402^{+0.050}_{-0.050}$	$0.0346^{+0.0072}_{-0.0070}$	$0.0033^{+0.0010}_{-0.0010}$
	$\zeta = 0$	$6.8^{+1.5}_{-1.5}$	$1.25^{+0.42}_{-0.42}$	$0.22^{+0.11}_{-0.11}$
	$\zeta = -1$	$27.4^{+5.9}_{-5.9}$	$5.0^{+1.7}_{-1.7}$	$0.89^{+0.44}_{-0.43}$
Muon channel				
Data		35	3	1
SM Background		$26.1^{+4.4}_{-4.3}$	$2.35^{+0.70}_{-0.60}$	$0.33^{+0.16}_{-0.12}$
W'	$M_{W'} = 2.5$ TeV	$48.7^{+4.1}_{-4.1}$	$36.1^{+2.8}_{-3.1}$	$20.3^{+3.0}_{-3.4}$
	$M_{W'} = 3$ TeV	$9.88^{+0.99}_{-0.98}$	$7.33^{+0.64}_{-0.65}$	$5.00^{+0.16}_{-0.39}$
HNC-CI	$\Lambda = 9$ TeV	$42.4^{+3.8}_{-3.8}$	$13.8^{+2.0}_{-2.0}$	$4.47^{+0.90}_{-0.94}$
	$\Lambda = 4$ TeV	1091^{+97}_{-98}	356^{+50}_{-52}	115^{+23}_{-24}
DM vector-coupling, $M_\chi = 50$ GeV, $\Lambda = 300$	$\zeta = +1$	$0.271^{+0.070}_{-0.067}$	$0.0151^{+0.0061}_{-0.0056}$	$0.00088^{+0.00051}_{-0.00043}$
	$\zeta = 0$	$6.7^{+1.6}_{-1.6}$	$1.43^{+0.54}_{-0.51}$	$0.31^{+0.17}_{-0.15}$
	$\zeta = -1$	$27.1^{+6.6}_{-6.5}$	$5.8^{+2.2}_{-2.1}$	$1.25^{+0.68}_{-0.60}$

6.3 Higher-order corrections for SM W boson background

The W boson, particularly through the off-shell tail of its M_T distribution, contributes an important and irreducible background in this analysis. An accurate prediction of the W boson's off-shell tail is also needed to establish the effects of interference with the signal. Therefore,

higher-order electroweak (EW) and QCD corrections are evaluated, binned in M_T :

$$K(M_T) = \frac{\Delta\sigma(\text{NLO})/\Delta M_T}{\Delta\sigma(\text{LO})/\Delta M_T}. \quad (4)$$

The NLO EW corrections, calculated with the HORACE [77] event generator using the CT10 [78] PDF set, depend strongly on M_T . While the corresponding K-factor is around 1.0 for transverse masses of 300 GeV, it decreases to around 0.5 for $M_T = 2.5$ TeV. The QCD corrections are calculated with MC@NLO, also using the CT10 PDF set, and are less M_T dependent, leading to a K-factor ranging from around 1.4 to 1.2. The impact of both these corrections is illustrated in Fig. 8. Also shown is the influence of the PDF set using the LO generator PYTHIA comparing CT10 and CTEQ6L1 [48].

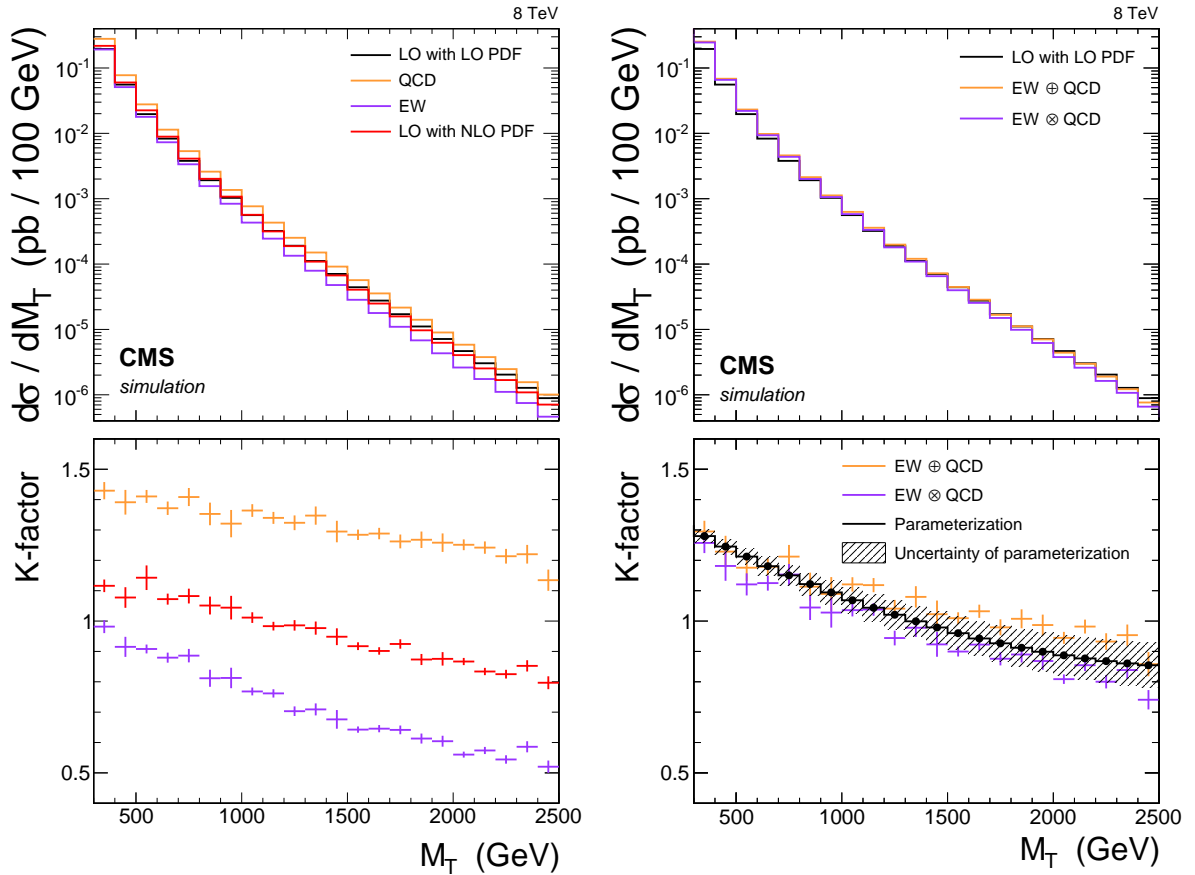


Figure 8: Electroweak and QCD corrections to the SM W-boson background prediction. Left: QCD and electroweak contributions compared to the LO calculation with LO PDF. Right: Combination of higher-order corrections with an additive and a multiplicative approach compared to the LO calculation with LO PDF, as well as a parameterization of the mean of the values obtained by the two methods. To derive the K-factor data on the right plot, one divides the sum or product of the K-factors on the left plot by the NLO/LO PDF K-factor.

To combine the EW and QCD differential cross sections, two different approaches have been used [79]: an additive or a multiplicative combination. As both, the EW and QCD K-factor include the NLO PDF information, a correction must be made to not account for the NLO PDF

twice. The combined K-factors are calculated by:

$$\begin{aligned}
 K_{\text{QCD} \oplus \text{EW}}^{\text{CT10}} &= \frac{\left[\frac{\Delta\sigma}{\Delta M_T} \right]_{\text{QCD}}^{\text{CT10}} + \left[\frac{\Delta\sigma}{\Delta M_T} \right]_{\text{EW}}^{\text{CT10}} - \left[\frac{\Delta\sigma}{\Delta M_T} \right]_{\text{LO}}^{\text{CT10}}}{\left[\frac{\Delta\sigma}{\Delta M_T} \right]_{\text{LO}}^{\text{CTEQ6L1}}}, \\
 K_{\text{QCD} \otimes \text{EW}}^{\text{CT10}} &= \frac{\left[\frac{\Delta\sigma}{\Delta M_T} \right]_{\text{QCD}}^{\text{CT10}}}{\left[\frac{\Delta\sigma}{\Delta M_T} \right]_{\text{LO}}^{\text{CTEQ6L1}}} \times \frac{\left[\frac{\Delta\sigma}{\Delta M_T} \right]_{\text{EW}}^{\text{CT10}}}{\left[\frac{\Delta\sigma}{\Delta M_T} \right]_{\text{LO}}^{\text{CTEQ6L1}}} \times \frac{\left[\frac{\Delta\sigma}{\Delta M_T} \right]_{\text{LO}}^{\text{CTEQ6L1}}}{\left[\frac{\Delta\sigma}{\Delta M_T} \right]_{\text{LO}}^{\text{CT10}}},
 \end{aligned} \tag{5}$$

where $\left[\frac{\Delta\sigma}{\Delta M_T} \right]$ is the differential cross section, the upper index gives the PDF set name and the lower index gives the type of correction applied.

Their effects differ by around 10%. The K-factor assumed in this analysis is obtained by taking the average of the two approaches, and treating half of their difference as a systematic uncertainty.

The means of the K-factors resulting from these two approaches are shown in Fig. 8 (right), with the distribution parametrized using a second-order polynomial. These higher-order corrections have a significant influence on the final result. This treatment represents an improvement over previous analyses [21–23], in which a constant K-factor of 1.3 was used across the whole M_T spectrum. For $M_T \geq 1.5$ TeV the value used in this analysis is closer to ~ 0.9 , as shown in the figure. This reduces the expected background, while leaving the signal unchanged since corresponding EW corrections have not been calculated.

6.4 Multijet background estimation from data

As stated in Section 6.1, the misidentification of jets as leptons, which is more likely for electrons than for muons, is a possible source of background for this search. While the contribution of QCD multijet events to the muon channel is negligible, a small contribution to the electron channel remains. In the latter channel, the shape and normalization of the QCD multijet background, as shown in Fig. 5 and used for the final results, is derived from data.

A QCD template is obtained from the events in which the electron candidate fails the isolation requirement but where all other event requirements are met. QCD template events are scaled with normalization factors from an independent control region, which is defined by the requirement $1.5 < E_T/E_T^{\text{miss}} < 10$. In this region, the ratio r_{tll} of ‘tight’ events (electron candidate passes all requirements of a well-isolated electron) to ‘loose’ events (all events in the region) is measured as a function of E_T and η . The resulting normalization factor for QCD template events is $r_{\text{tll}}/(1 - r_{\text{tll}})$. Contributions from processes with genuine electrons or photons are estimated via simulation and are subtracted. They amount to 4–13% of the loose event counts, the most important contributions being W+jets and γ +jets events, along with small contributions from $t\bar{t}$, single top-quark, Drell–Yan, and dibosons. This results in ratios of ‘tight’ to ‘loose’ event counts varying from 7% in the barrel to 25% in the very forward region, for electrons with $E_T > 200$ GeV. Based on a set of cross-checks, a total uncertainty of 40% is assigned to the multijet background.

7 Systematic uncertainties

Mismeasurement of lepton energy or momentum, resulting from both detector resolution and imperfect scale calibration, will result in a smearing of the M_T spectrum. For each source of

uncertainty, shifts of $\pm 1\sigma$ are applied, the kinematics of the objects ($e, \mu, E_T^{\text{miss}}$) are recalculated, as well as M_T , and the kinematic selection is reapplied. The resulting distribution is parameterized, and the difference with respect to the original parameterization is used to estimate the systematic uncertainty in the number of background events. The total uncertainty of the expected background is indicated in Fig. 5 and specified in Table 5.

The systematic uncertainty in the electron energy scale is estimated to be 0.4 (0.8)% in the barrel (endcaps). For the electron energy resolution uncertainty, an additional Gaussian smearing of 1.2 (2.4)% for the barrel (endcap) region is applied to the MC simulation [27].

The muon transverse momentum scale uncertainty is estimated as $5\% \times p_T / \text{TeV}$. The momentum resolution uncertainty is taken into account by applying an additional smearing of 3.2% to the MC simulation. Both, scale and resolution uncertainty were estimated from the measurement of cosmic muons [29]. The uncertainty of the muon momentum measurement relates to the smallness of curvature of tracks for high- p_T muons, while the energy of the electrons is measured in the crystal calorimeter and the uncertainty is smaller.

As explained in Section 6.3 the difference between the two ways of combining the EW and QCD corrections is treated as the systematic uncertainty in the K-factor for W-boson production. The effect of even higher order corrections like Sudakov corrections is expected to be small and therefore not considered.

The ratio of data to MC efficiencies are the scale factors (SFs) defined in Section 4. The uncertainty due to the determination method and the extrapolation to high M_T is taken as the systematic uncertainty in the SFs.

The simulated distribution of pp collision vertices per bunch-crossing has to be reweighted to the distribution measured in data. The uncertainty due to this reweighting method is treated as the systematic uncertainty of the pileup simulation. The effect on the background event yield due to this uncertainty is smaller than 1%.

The overall uncertainty in the determination of E_T^{miss} in each event is derived from the individual uncertainties assigned to the objects (jets, e, μ, τ, γ , and unclustered energy) used by the particle-flow algorithm. The contribution of each object type is varied according to its uncertainty. This uncertainty is propagated to the particle-flow E_T^{miss} [64]. The quadratic sum of the individual uncertainties gives the overall uncertainty in the particle-flow E_T^{miss} . To account for correlations, the E_T^{miss} uncertainty components that are also used for the lepton (e.g. electron energy scale and resolution in the electron channel) are not included in the E_T^{miss} distributions of Fig. 9 but are included in their respective distributions.

The theoretical uncertainty related to the choice of the PDF set was estimated using the PDF4LHC recommendation [80, 81], reweighting the background samples with three different PDF sets: NNPDF2.3 [82], MWST2008 [83], CT10 [78]. For each central PDF set an uncertainty band is derived from the different error PDF sets. The error PDF sets describe the uncertainties of the PDF set including uncertainties due to α_s variation. The envelope of these three error bands is then taken as the uncertainty due to the choice of PDF set. The same procedure was used for the signal cross section predictions.

For the multijet background prediction, the uncertainties described in Section 6.4 are used.

The accuracy of the integrated luminosity estimate is 2.6% [25].

An estimate of the uncertainty in the number of background events in the M_T spectrum arising from the uncertainties described above, but not including the luminosity uncertainty, is shown

in Fig. 9. The dominant systematic uncertainties are due to the PDF sets in the electron channel and due to momentum scale uncertainty in the muon channel.

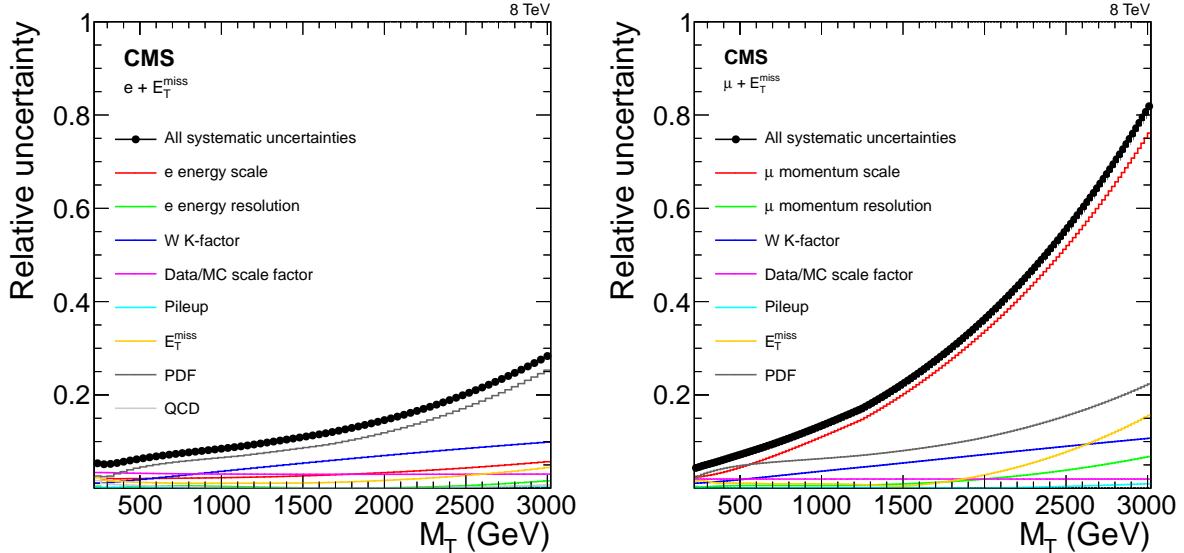


Figure 9: Individual contributions of relative systematic uncertainties on the background event yields in the electron (left) and muon (right) channels.

8 Limit-setting procedures

As no significant deviation from predictions is seen in the M_T distribution, exclusion limits on new signals can be set. Upper limits on the production cross section times branching fraction $\sigma_{W'} \mathcal{B}(W' \rightarrow \ell \nu)$, with $\ell = e$ or μ , are determined using a Bayesian method [56] with a uniform positive prior probability distribution for the signal cross section. Systematic uncertainties on the expected signal and background yields are included via nuisance parameters with log-normal prior distributions.

To determine a model independent upper limit on the cross section times branching fraction, all events above a threshold M_T^{\min} are summed. From the number of background events, signal events, and observed data events, the cross section limit can be calculated. No assumptions on the shape of the signal M_T distribution have to be made. This method has a good sensitivity, comparable to a multi-bin approach, when the background is low.

For the limits on the SSM W' , HNC-CI, DM, split-UED, and TeV^{-1} models, the entire M_T spectrum as displayed in Fig. 5 with $M_T > 220$ GeV selection is considered, taking the shape of the distribution into account using a binned likelihood (multi-bin counting). This is performed for different values of the model parameters of each signal, resulting in limits in terms of these model parameters, such as the W' boson mass or the interaction scale Λ .

The analyses of the SSMS and SSMO hypotheses are technically challenging, as the number of events in an M_T region can be larger or smaller than predicted by the standard model. For the SSMS model, the W - W' -boson production cross section would be reduced with respect to the standard model W boson, as seen in Table 2, affecting the M_T range below the Jacobian peak as shown in Fig. 3 (top left). An assumption of the overall cross section always influences the whole signal distribution. However, the effect of the SSMS and SSMO signal compared to the SM expectation is to reduce the observed event count in one region, while increasing it in another. This makes the analysis less sensitive in setting a cross section limit. The W' boson

coupling strength $g_{W'}$ has therefore been chosen as a free parameter for the models including W - W' interference (SSMS and SSMO). A smaller coupling will result in a narrower Jacobian peak, as well as less modulation in the interference region.

The limits on the W' boson coupling strength in the SSMS and SSMO scenarios have been determined using the modified-frequentist CL_s method [84, 85]. The test statistic used is

$$q_\mu = -2 \ln \frac{\mathcal{L}(\text{data}|\mu, \hat{\theta}_\mu)}{\mathcal{L}(\text{data}|0, \hat{\theta}_0)}, \quad (6)$$

where \mathcal{L} is the likelihood, μ is the parameter of interest (here, the coupling), and $\hat{\theta}$ is the set of nuisance parameters maximizing the likelihood.

9 Interpretation of the results

This section discusses the limits established for the various models summarized in Table 1. All limits presented here are at 95% CL unless stated otherwise. Note that all presented mass limits come with a lower bound of $M_T = 220$ GeV, below which background dominates the M_T distribution.

9.1 Model-independent cross section limit

Apart from the model-dependent multi-bin limits, a model-independent cross section limit is determined using a single bin ranging from a lower threshold on M_T to infinity, with the results shown in Fig. 10 for the individual electron and muon channels and Fig. 11 for the combination of both channels. Only model-independent contributions to signal efficiencies, e.g., the lepton reconstruction efficiency including detector acceptance, are considered, derived using the simulated $W \rightarrow \ell\nu$ sample. The signal efficiencies are estimated to be 86% in the muon channel and 83% in the electron channel.

In order to determine any limit for a specific model from the model-independent limit shown here, only the model-dependent part of the efficiency must be taken into account. This means an efficiency A describing the effect on the signal of the M_T^{\min} threshold and of the two kinematic selection criteria, $0.4 < p_T/E_T^{\text{miss}} < 1.5$ and $\Delta\phi(\ell, \vec{p}_T^{\text{miss}}) > 2.5$ (see Section 4), must be determined. The p_T and E_T^{miss} measurements are affected dominantly by the lepton resolutions, as described in Section 2. Multiplying A with the theoretical cross section σ and the branching fraction \mathcal{B} , the result can be compared with an exclusion limit from Figs. 10 or 11. Values of $\sigma \times \mathcal{B} \times A$ larger than the limit indicated by the solid line can be excluded. To find the best value of M_T^{\min} , the threshold should be optimized with respect to the expected limit.

The electron channel is more sensitive than the muon channel, as the energy resolution is superior. In the muon channel, shown in Fig. 10 (right), a small excess of events yields a larger and therefore worse observed limit for most values of M_T^{\min} compared to the expectation. The step-like structure for high transverse mass thresholds corresponds to the small discrete numbers of events in these regions.

9.2 Limits on an SSM W' boson

The search for an SSM W' boson yields limits on the cross section times branching fraction for the electron and muon channels. The multi-bin method is used to determine the 95% CL upper cross section limits, as shown in Fig. 12. The indicated theoretical cross sections are the NNLO values for lepton+ E_T^{miss} channel, as detailed in Section 3, and are the same for both

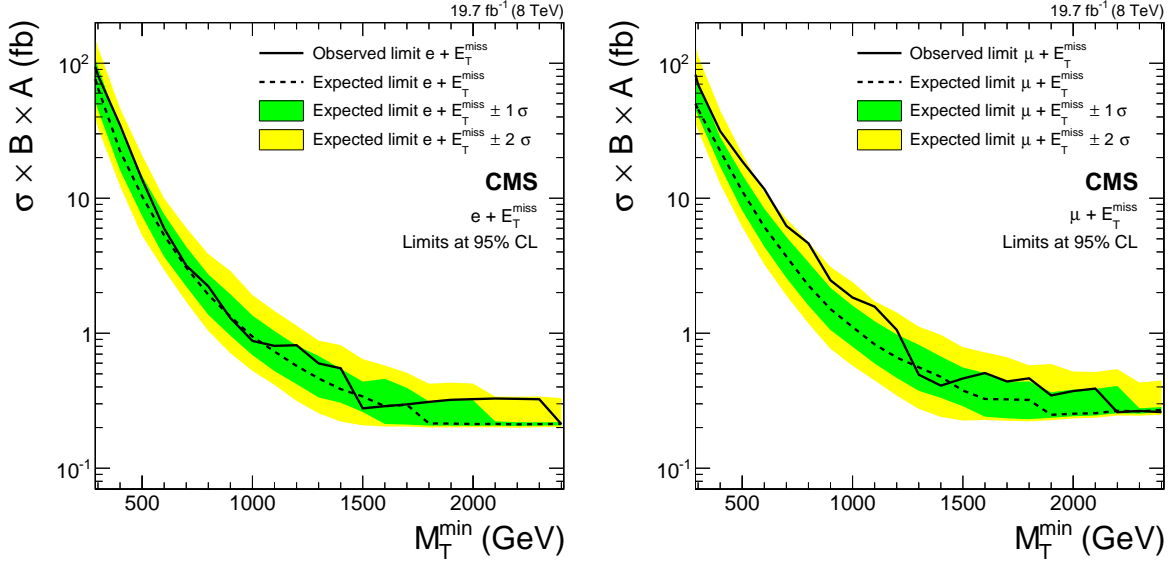


Figure 10: Cross section upper limits at 95% CL on the effective cross section $\sigma(W') \mathcal{B}(W' \rightarrow \ell\nu)A$ above a threshold M_T^{\min} for the individual electron and muon channels. Shown are the observed limit, expected limit, and the expected limit 1σ and 2σ intervals. Only detector acceptance is taken into account for the signal. The parameter A describes the efficiency derived from the kinematic selection criteria and the M_T^{\min} threshold.

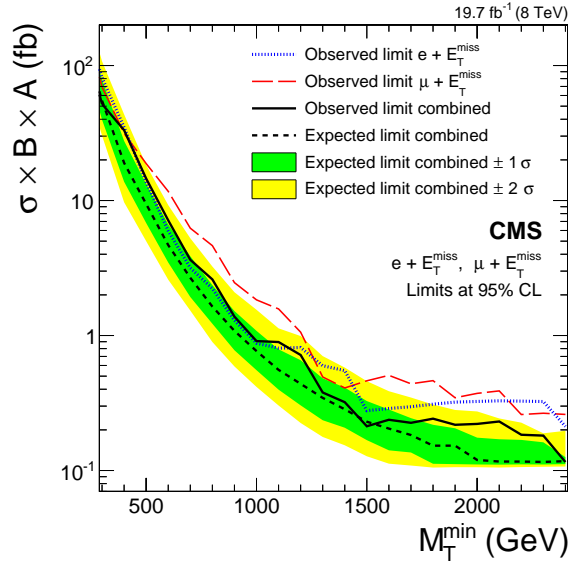


Figure 11: Cross section upper limits at 95% CL on the effective cross section $\sigma(W') \mathcal{B}(W' \rightarrow \ell\nu)A$ above a threshold M_T^{\min} for the combination of the electron and muon channels. Shown are the observed limits of the electron channel, muon channel, and the combination of both channels and the combined expected limit, together with the combined expected limit 1σ and 2σ intervals. Only detector acceptance is taken into account for the signal. The parameter A describes the efficiency derived from the kinematic selection criteria and the M_T^{\min} threshold.

channels. The PDF uncertainties are shown as a thin band around the NNLO cross section. The central value of the theoretical cross section times branching fraction is used for deriving the mass limit. The existence of an SSM W' boson of mass less than 3.22 TeV (compared with an expected limit of 3.18 TeV) in the electron channel, and 2.99 TeV (compared with an expected limit of 3.09 TeV) in the muon channel, is excluded. The electron channel has a slightly higher expected sensitivity because of its better resolution.

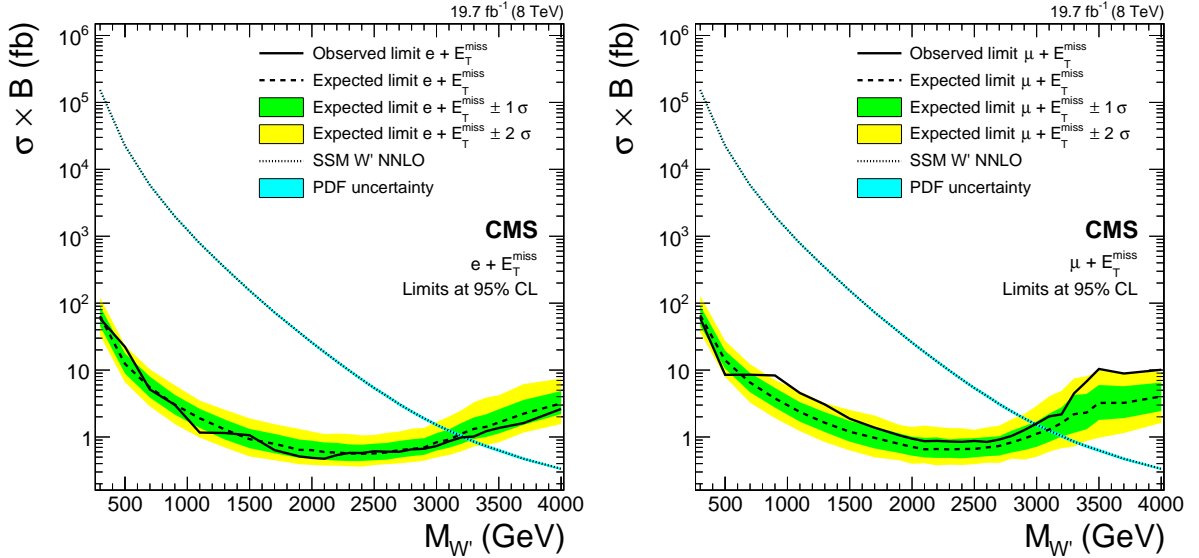


Figure 12: Upper limits at 95% CL on $\sigma(W') \mathcal{B}(W' \rightarrow \ell\nu)$ with $\ell = e$ (left) and $\ell = \mu$ (right). Shown are the theoretical cross section, the observed limit, the expected limit, and the expected limit 1σ and 2σ intervals. The theoretical cross section incorporates a mass-dependent NNLO K-factor.

Limits can also be obtained for the combined electron and muon channels. Uncertainties deriving from the lepton identification efficiencies for each channel are assumed to be independent. Uncertainties due to the E_T^{miss} determination, pileup estimate, and luminosity measurement are each assumed to be fully correlated between the channels. Combining both channels, which corresponds to doubling the event count, increases the mass limit to 3.28 TeV (compared with an expected limit of 3.26 TeV). This compares with the previously established combined limit of 2.5 TeV [23], which is based on an integrated luminosity of 5 fb^{-1} at $\sqrt{s} = 7 \text{ TeV}$. Figure 13 displays the excluded W' cross section times branching ratio as a function of the W' -boson mass. The corresponding values are summarized in Table 6.

If the cross section limits are compared to the LO cross section, the SSM W' mass limits change slightly to 3.16 TeV (compared with an expected limit of 3.14 TeV) for the electron channel, 2.96 TeV (compared with an expected limit of 3.04 TeV) for the muon channel, and 3.25 TeV (compared with an expected limit of 3.21 TeV) for the combination of both channels.

Table 6: Upper cross section limits at 95% CL for various SSM W' boson masses, based on the combination of the electron and muon channels.

$M_{W'}$ (GeV)	300	1100	1500	2000	3000	3500	4000
Expected limit (fb)	48	1.4	0.69	0.42	0.56	1.4	2.3
Observed limit (fb)	39	1.6	1	0.4	0.69	1.6	1.9

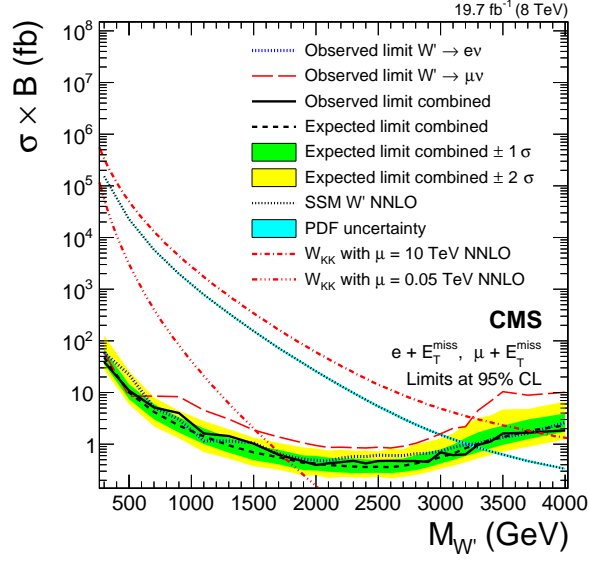


Figure 13: Limits for heavy W' bosons for the electron and the muon channels, and for the two channels combined. Shown are the theoretical cross section for the SSM and two split-UED scenarios, the observed limit, the expected limit, and the expected limit 1σ and 2σ intervals. The theoretical cross sections incorporate a mass-dependent NNLO K-factor. The PDF uncertainties for the SSM are shown as a light blue band around the cross section curve. For the split-UED scenarios, the PDF uncertainties are expected to be small, similar to the uncertainty in the SSM scenario.

9.3 Interpretation in the HNC-CI model

Another interpretation of the observed data can be made in the framework of the HNC-CI model, providing a limit on the contact interaction scale Λ . The statistical interpretation is identical to that for an SSM W' boson, using a Bayesian multi-bin approach with a uniform prior for the signal cross section [56]. The difference in shape with respect to the W' Jacobian peak does not affect the limit-setting procedure. The cross section scales as Λ^{-4} . The shape and signal efficiency, however, are independent of Λ , leading to the constant expected and observed limits shown in Fig. 14. The limit on Λ is calculated to be 11.3 TeV in the electron and 10.9 TeV in the muon channel. In the considered model the contact interaction must be flavor symmetric for $\Lambda < 500$ TeV [2]. Combining both channels, a limit on Λ of 12.4 TeV is observed and 13.6 TeV is expected.

9.4 Dark matter interpretation

The data may be interpreted in the context of an effective dark matter theory. The search presented is inclusive, meaning that it includes final states of lepton+ E_T^{miss} and well as lepton+ E_T^{miss} +jet, since no event selection criteria based on jets are applied. The statistical interpretation is a Bayesian approach with a uniform prior [56], based on the multi-bin approach. In order to be comparable to other dark matter searches, the limits in this model are determined at 90% CL. Electron and muon channels are combined, since the recoiling W boson is a standard model boson, for which the decay channel should not depend on the new physics model. Vector-like (spin-independent) and axial-vector-like (spin-dependent) couplings are considered.

The exclusion limits are determined as cross section limits (see Fig. 15) which are subsequently transformed into limits on the effective scale parameter Λ as a function of M_{χ} , as shown in Fig. 16. In order to compare these collider limits with results from direct detection experiments,

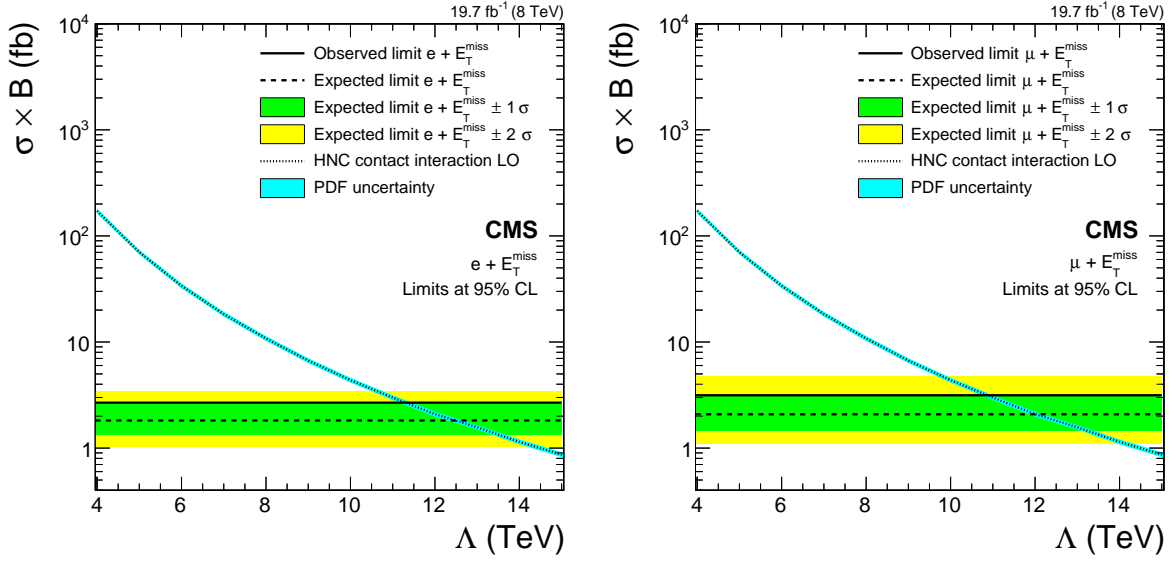


Figure 14: Upper limits at 95% CL on $\sigma\mathcal{B}(\text{pp} \rightarrow \ell\nu)$ with $\ell = e$ (left) and $\ell = \mu$ (right) in terms of the contact interaction scale Λ in the HNC-CI model.

they are translated into limits on the DM-proton cross section, shown in Fig. 17. We recalculate the excluded nucleon cross section for a given Λ and M_χ using the conversion formula with interference from Ref. [86].

The collider cross section limits in Fig. 15 show that the excluded cross section is flat as a function of M_χ , as expected since the signal kinematics do not change appreciably for different M_χ . The coupling does not have a large effect on the limit. The different interference scenarios have a visible influence on the limit. In the case of $\zeta = +1$, a cross section greater than 0.6 pb is excluded, whereas for $\zeta = 0$ and for $\zeta = -1$ the cross section limit is 0.05 pb. For high M_χ the phase space to produce two heavy particles and a W boson is small, therefore the signal cross section is reduced and its shape more consistent with the background. These effects yield a reduced sensitivity at this center-of-mass energy.

As the M_T distributions for vector-like (spin-independent) and axial-vector-like (spin-dependent) couplings are very similar, the derived limits for the two cases do not differ substantially.

For lower masses a constant Λ exclusion is obtained for $M_\chi \leq 100$ GeV of $\Lambda < 300$ GeV for $\zeta = +1$, $\Lambda < 700$ GeV for $\zeta = 0$, and $\Lambda < 1000$ GeV for $\zeta = -1$. The difference between vector-like and axial-vector-like couplings is small for low M_χ for all three values of ζ , but a difference is observed in the high- M_χ region, above 100 GeV. An overview is given in Fig. 16.

For comparison the limit from the monojet final state [53] is shown. The conversion to χ -proton cross section depends on the coupling parameter ζ , although the monojet analysis is not sensitive to ζ . The limits determined from the direct detection experiments depend on different model assumptions [87]. Therefore we do not give a direct comparison here.

The χ -proton cross section upper limits at 90% CL for $M_\chi = 10$ GeV are presented in Table 7 and Fig. 17.

9.5 Limits on coupling strength in models with interference

Limits on the W' boson models, taking into account interference effects with the W boson, are set on the W' coupling $g_{W'}$ in terms of the SM W -boson coupling strength g_W . The corresponding impact on the observable distribution is modeled using a reweighting technique. Thus,

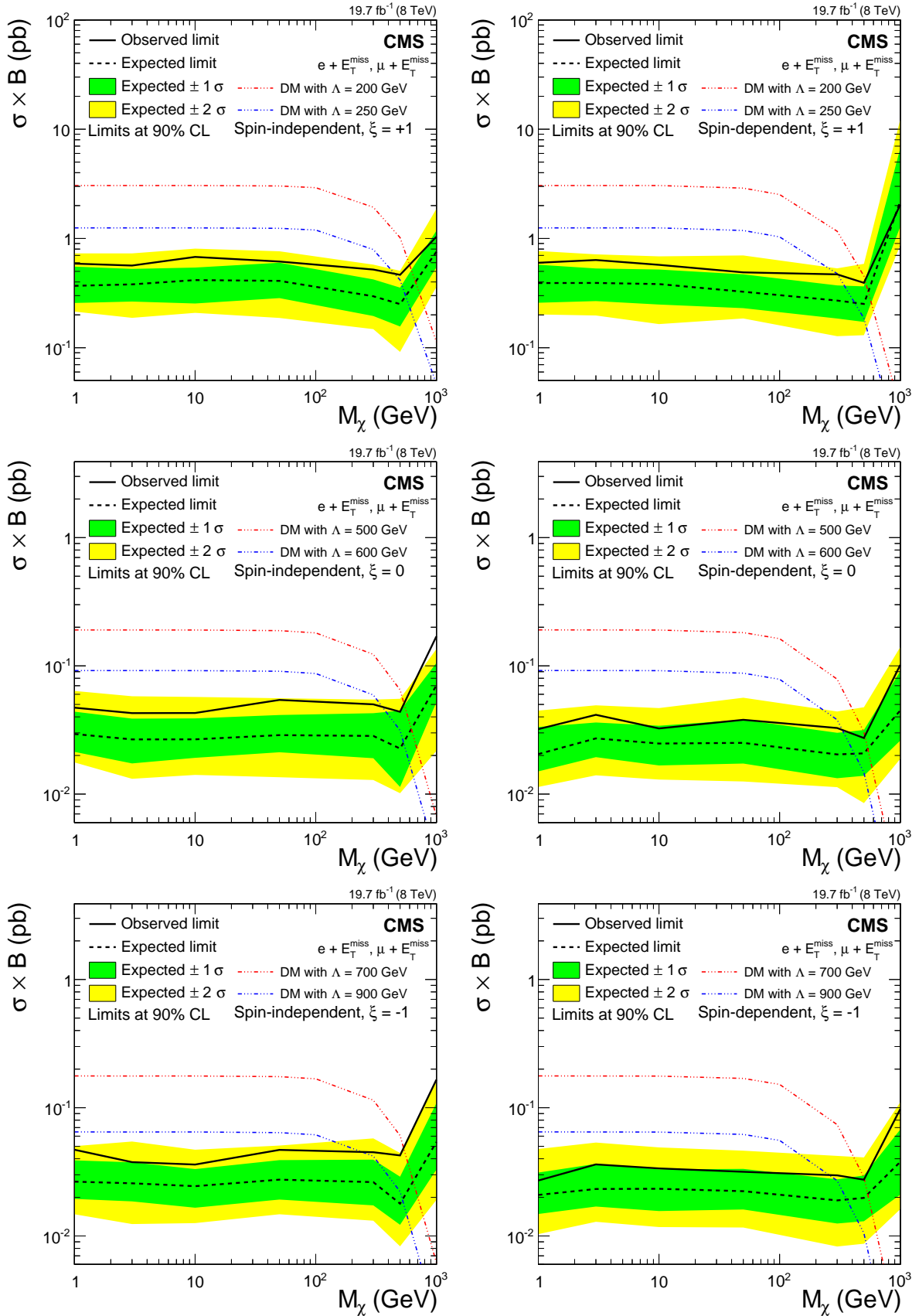


Figure 15: Upper limits on $\sigma \mathcal{B}(pp \rightarrow \chi\chi\ell\nu)$ for vector-like (spin-independent, left column) and axial-vector-like (spin-dependent, right column) couplings. Limits are calculated for the cases (from top to bottom) $\xi = +1, 0$ and -1 . Note the different vertical scales.

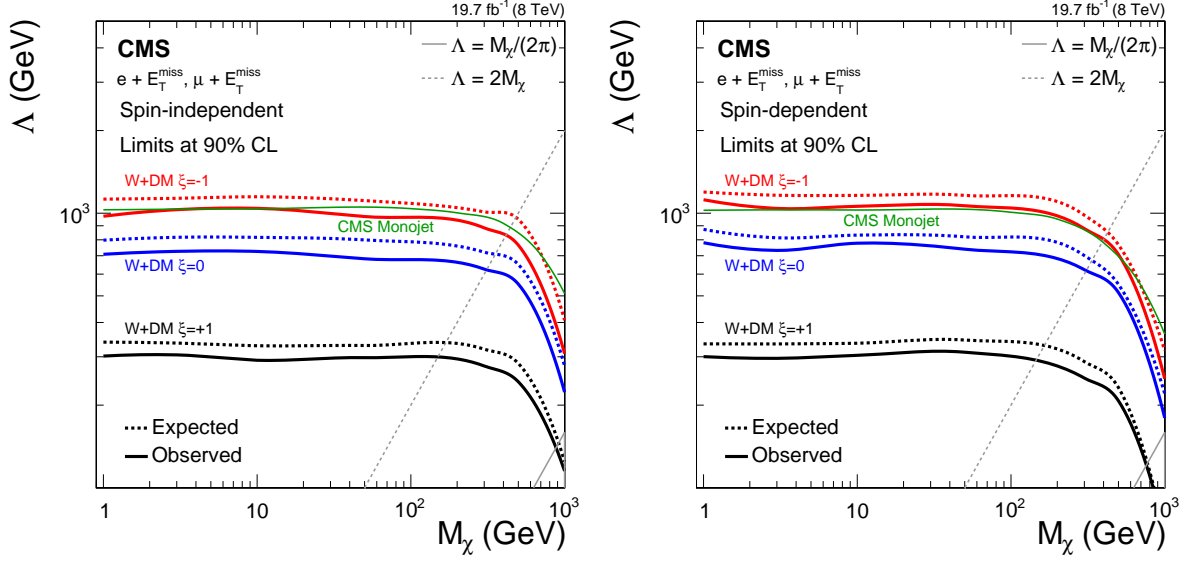


Figure 16: Exclusion plane in Λ - M_χ , for the combination of the electron and muon channels. Vector-like (left) and axial-vector-like (right) couplings are shown. The two gray lines indicate where the coupling becomes non-perturbative and (g_{DM}) is equal to 1, as described in Section 3.3. The green line shows the limit in the monojet final state [53], which is independent of ξ for the limit on Λ .

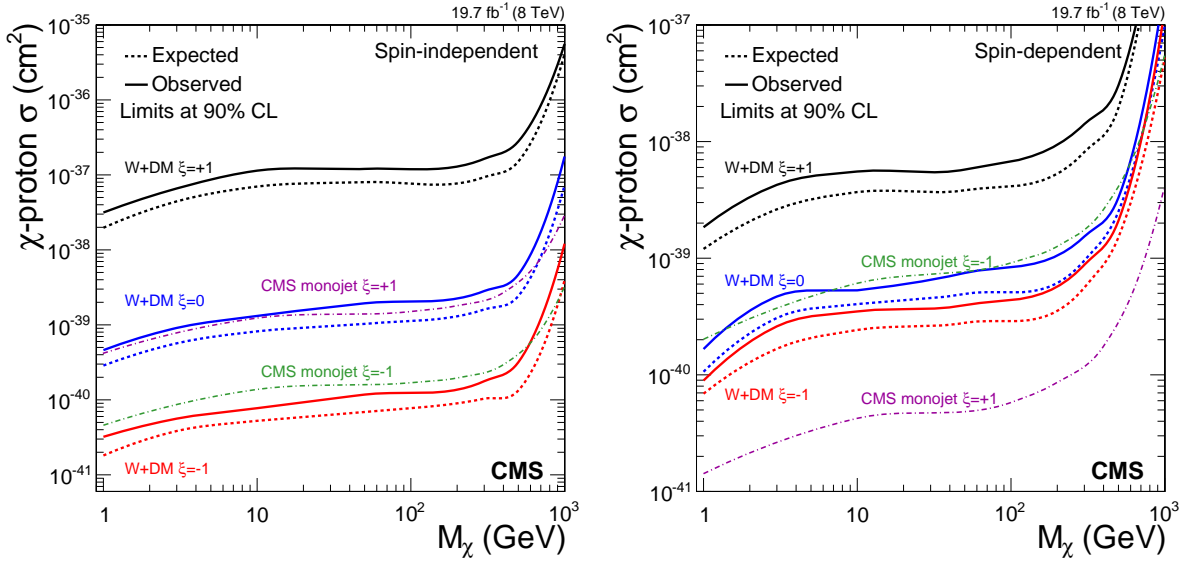


Figure 17: Excluded proton-dark matter cross section for vector-like (left) and axial-vector-like (right) couplings, for the combination of the electron and muon channels. For comparison the result from the monojet DM search [53] is also shown.

Table 7: The χ -proton cross section upper limits at 90% CL for $M_\chi = 10$ GeV.

ξ	Vector coupling (cm^2)	Axial-vector coupling (cm^2)
-1	4×10^{-41}	1×10^{-40}
0	6×10^{-40}	2×10^{-40}
+1	3×10^{-38}	2×10^{-39}

effects such as the influence on the decay width and the impact on interference by the altered coupling are taken into account, as shown in Fig. 3 (middle right). The following interference occurs in the mass range between M_W and $M_{W'}$. If the coupling of the W' boson has the same sign (SSMS) with respect to the W -boson coupling to left-handed fermions, the interference effect is destructive; in case of opposite sign (SSMO) coupling, it is constructive. For $M_T > M_{W'}$ the effect is vice-versa.

The limit on the coupling strength $g_{W'}$ as a function of the W' -boson mass is shown in Fig. 18. The mass limits in the case where the W' -boson coupling is equal to the W -boson coupling are summarized in Table 8.

Table 8: Summary of all SSMS and SSMO exclusion limits on the W' -boson mass in the electron and muon channels, and for their combination assuming $g_W = g_{W'}$.

Model	Channel	Observed lower limit (TeV)	Expected lower limit (TeV)
SSMS	e	3.41	3.52
SSMS	μ	3.97	3.43
SSMS	combined	4.00	3.83
SSMO	e	3.54	3.57
SSMO	μ	3.22	3.38
SSMO	combined	3.71	3.83

9.6 Interpretation in the split-UED model

The observed limits on the SSM W' boson (see Section 9.2) can be reinterpreted as limits on the $W_{\text{KK}}^{(2)}$ mass in the framework of split-UED, with the second KK excitation being the only accessible state at present LHC energies with non-zero couplings to SM particles. Figure 13 shows two examples of $W_{\text{KK}}^{(2)}$ -boson mass limits for values of the bulk mass parameter $\mu = 0.05$ TeV and $\mu = 10$ TeV. For these two examples, the lower mass limit is 1.74 TeV for $\mu = 0.05$ TeV and 3.71 TeV for $\mu = 10$ TeV, when combining both channels. The lower limits on the mass can be directly translated into bounds on the split-UED parameter space $(1/R, \mu)$ as shown in Fig. 19.

9.7 Interpretation in the TeV^{-1} model

Based on the model-independent cross section limit and the recipe described in Section 9.1, a single-bin limit on the compactification scale M_C of the TeV^{-1} model is derived using the kinematic selection efficiency for this particular model. The lower bound on M_C is established as 3.4 TeV. The existing indirect limit on M_C is 6.8 TeV, which was obtained by fitting results from LEP2, Tevatron, and HERA experiments [88]. The lower limit set by LEP2 experiments is 6.6 TeV, which is the dominant contribution. The sensitivity of this analysis is therefore still less stringent than that based on LEP2 data.

10 Summary

A search for physics beyond the standard model, based on events with a final state containing a charged lepton (electron or muon) and significant missing transverse energy, has been performed, using proton-proton collision data at $\sqrt{s} = 8$ TeV, corresponding to an integrated luminosity of 19.7 fb^{-1} . No significant deviation from the standard model expectation has been observed in the transverse mass distribution.

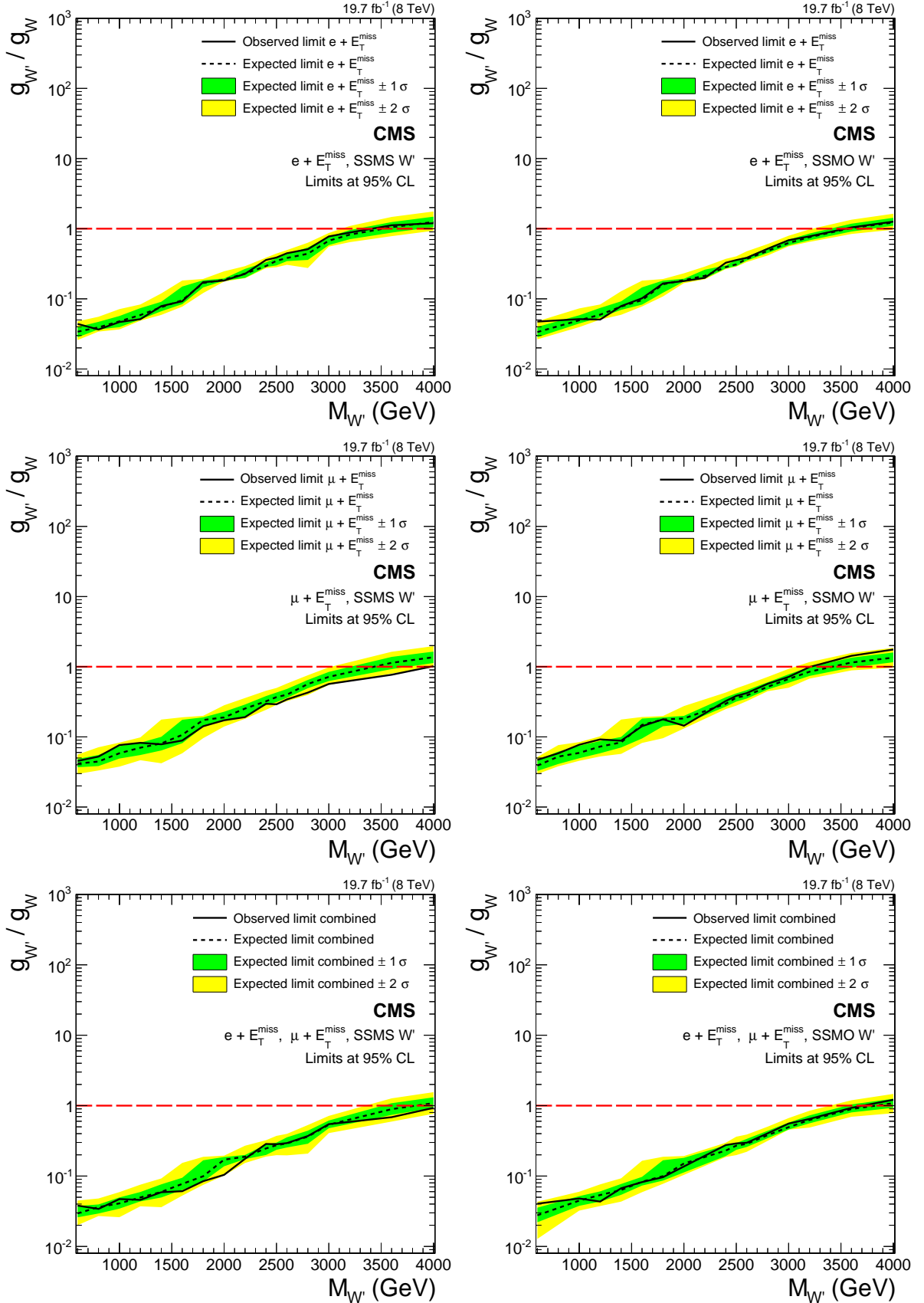


Figure 18: Limits on the coupling $g_{W'}$ in terms of the SM coupling g_W in the electron (top row) and muon (middle row) channels, and their combination (bottom row). Limits for the SSMS model are displayed in the left column, those for the SSMO model in the right column.

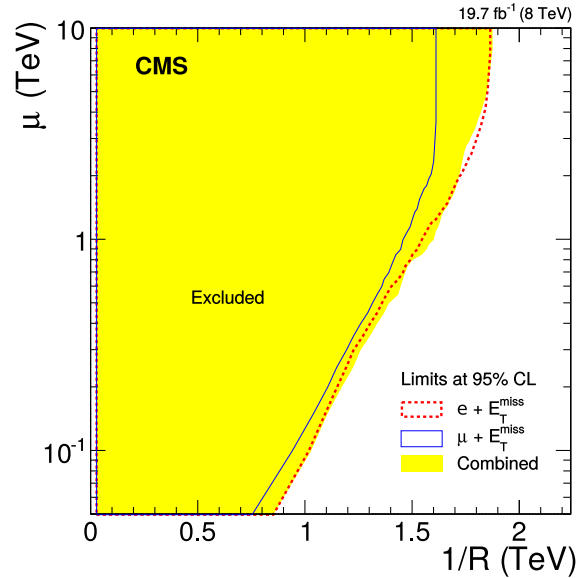


Figure 19: Limits on the split-UED parameters μ and $1/R$, derived from the W' -boson mass limits, taking into account the corresponding width of the $W_{\text{KK}}^{(2)}$ boson.

A model-independent upper limit at 95% CL on the cross section times branching fraction of additional contributions has been established, ranging from 100 to 0.1 fb over an M_T range of 300 GeV to 2.5 TeV, respectively. The results have been interpreted in the context of various models, as summarized below.

An SSM W' boson that does not interfere with the W boson has been excluded at 95% CL for W' -boson masses up to 3.22 (2.99) TeV for the electron (muon) channel, where the expected limit is 3.18 (3.06) TeV. When combining both channels, the limit improves to 3.28 TeV. Lower mass limits in either channel are implicit due to trigger thresholds.

An interpretation in terms of a four-fermion contact interaction yields a limit for the compositeness energy scale Λ of 11.3 TeV in the electron channel, 10.9 TeV in the muon channel, and 12.4 TeV for their combination.

Assuming the production of a pair of dark matter particles along with a recoiling W boson that subsequently decays leptonically, the results have been reinterpreted in terms of an effective dark matter theory. The effective scale is excluded below 0.3 to 1 TeV, depending on model parameters. This is particularly interesting for low masses of dark matter particles, where the sensitivity of direct searches is poor.

Building upon earlier versions of this analysis [24], the expected impact of W - W' interference on the shape of the W boson M_T distribution is fully taken into account. Along with the shape, the expected cross section varies, making possible the setting of limits for models with both destructive (SSMS) and constructive (SSMO) interference.

The lower limit on the W' -boson mass is 3.41 (3.97) TeV in the electron (muon) channels for the SSMS and 3.54 (3.22) TeV for the SSMO. For the first time, limits in terms of generalized lepton couplings are given.

An interpretation of the search results has been made in a specific framework of universal extra dimensions where bulk fermions propagate in the one additional dimension. The second Kaluza–Klein excitation $W_{\text{KK}}^{(2)}$ has been excluded for masses below 1.74 TeV, assuming a bulk mass parameter μ of 0.05 TeV, or for masses below 3.71 TeV, for $\mu = 10$ TeV. In an alternative

model in which only SM gauge bosons propagate in a compactified extra dimension (TeV^{-1} model), a lower bound on the size of the compactified dimension, M_C , has been set at 3.40 TeV.

Study of the mono-lepton channel provides a powerful tool to probe for beyond the standard model physics. All the results of this search are summarized in Fig. 20, including the expected and observed limits. Fig. 20 is structured by theories and the related model parameters (particle mass, compositeness scale Λ or dark matter effective field scale Λ) as given in Table 1. The three representative signal examples (SSM W' , contact interaction and dark matter) are shown in the upper figure section. Limits for specific models along with the model independent cross section limit are given in the lower part of the figure.

Acknowledgments

We congratulate our colleagues in the CERN accelerator departments for the excellent performance of the LHC and thank the technical and administrative staffs at CERN and at other CMS institutes for their contributions to the success of the CMS effort. In addition, we gratefully acknowledge the computing centers and personnel of the Worldwide LHC Computing Grid for delivering so effectively the computing infrastructure essential to our analyses. Finally, we acknowledge the enduring support for the construction and operation of the LHC and the CMS detector provided by the following funding agencies: the Austrian Federal Ministry of Science, Research and Economy and the Austrian Science Fund; the Belgian Fonds de la Recherche Scientifique, and Fonds voor Wetenschappelijk Onderzoek; the Brazilian Funding Agencies (CNPq, CAPES, FAPERJ, and FAPESP); the Bulgarian Ministry of Education and Science; CERN; the Chinese Academy of Sciences, Ministry of Science and Technology, and National Natural Science Foundation of China; the Colombian Funding Agency (COLCIENCIAS); the Croatian Ministry of Science, Education and Sport, and the Croatian Science Foundation; the Research Promotion Foundation, Cyprus; the Ministry of Education and Research, Estonian Research Council via IUT23-4 and IUT23-6 and European Regional Development Fund, Estonia; the Academy of Finland, Finnish Ministry of Education and Culture, and Helsinki Institute of Physics; the Institut National de Physique Nucléaire et de Physique des Particules / CNRS, and Commissariat à l'Énergie Atomique et aux Énergies Alternatives / CEA, France; the Bundesministerium für Bildung und Forschung, Deutsche Forschungsgemeinschaft, and Helmholtz-Gemeinschaft Deutscher Forschungszentren, Germany; the General Secretariat for Research and Technology, Greece; the National Scientific Research Foundation, and National Innovation Office, Hungary; the Department of Atomic Energy and the Department of Science and Technology, India; the Institute for Studies in Theoretical Physics and Mathematics, Iran; the Science Foundation, Ireland; the Istituto Nazionale di Fisica Nucleare, Italy; the Korean Ministry of Education, Science and Technology and the World Class University program of NRF, Republic of Korea; the Lithuanian Academy of Sciences; the Ministry of Education, and University of Malaya (Malaysia); the Mexican Funding Agencies (CINVESTAV, CONACYT, SEP, and UASLP-FAI); the Ministry of Business, Innovation and Employment, New Zealand; the Pakistan Atomic Energy Commission; the Ministry of Science and Higher Education and the National Science Centre, Poland; the Fundação para a Ciência e a Tecnologia, Portugal; JINR, Dubna; the Ministry of Education and Science of the Russian Federation, the Federal Agency of Atomic Energy of the Russian Federation, Russian Academy of Sciences, and the Russian Foundation for Basic Research; the Ministry of Education, Science and Technological Development of Serbia; the Secretaría de Estado de Investigación, Desarrollo e Innovación and Programa Consolider-Ingenio 2010, Spain; the Swiss Funding Agencies (ETH Board, ETH Zurich, PSI, SNF, UniZH, Canton Zurich, and SER); the Ministry of Science and Technology, Taipei; the Thailand Center of Excellence in Physics, the Institute for the Promotion of Teach-

CMS

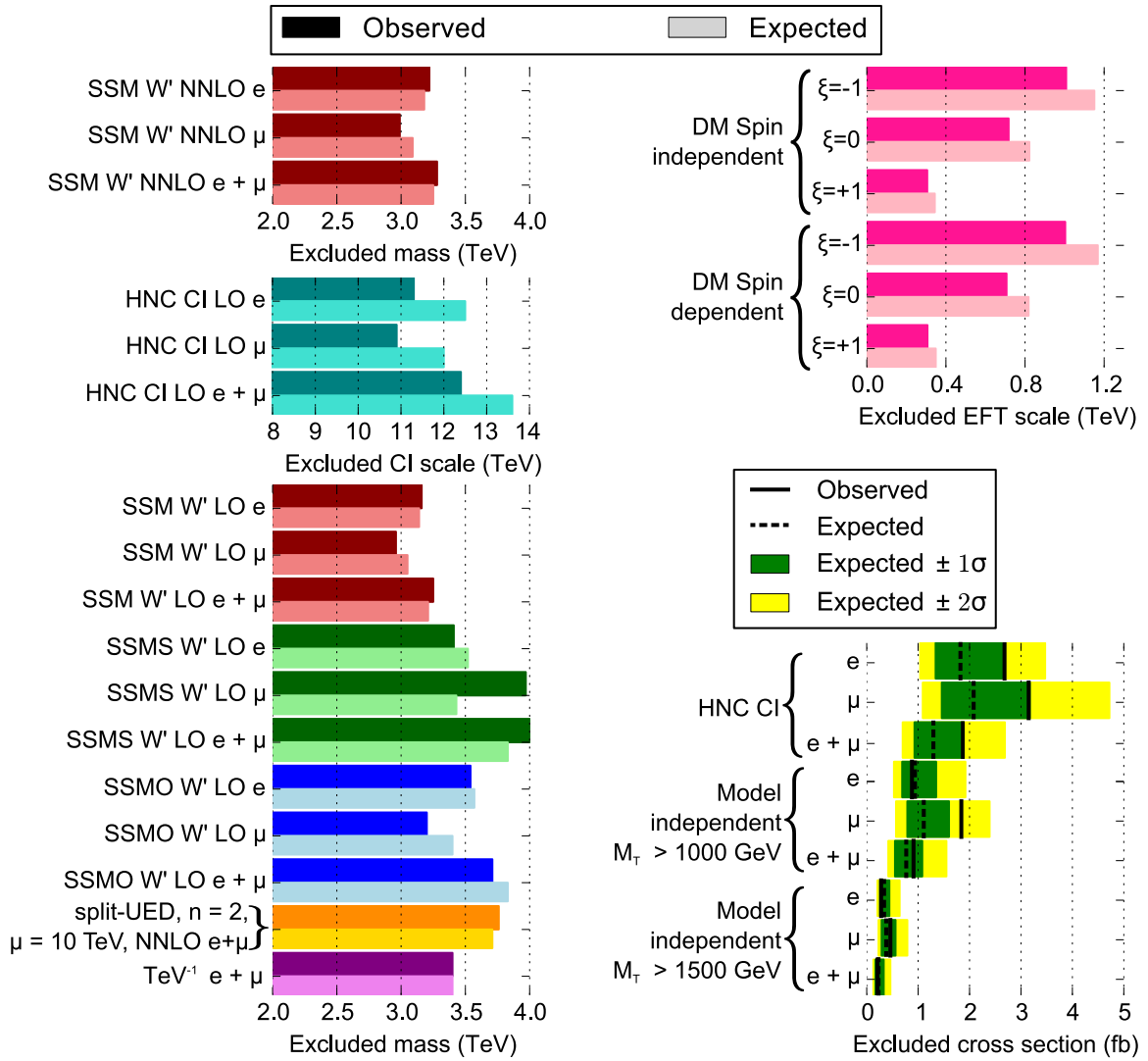
19.7 fb⁻¹ (8 TeV)

Figure 20: Summary of all exclusion limits in the electron and muon channels, and for their combinations. No interference of W' and W bosons is considered in the interpretation labeled as SSM while it is taken into account in the SSMS and SSMO models. For the HNC contact interaction, the compositeness scale Λ is probed. In the upper rows of the right column, the EFT limits are shown for the DM interpretations in term of Λ for small dark matter masses $M_\chi < 100$ GeV. The reinterpretation in terms of additional extra dimensions is provided in the context of split-UED, given for a bulk mass parameter $\mu = 10$ TeV, and in the TeV⁻¹ model.

ing Science and Technology of Thailand, Special Task Force for Activating Research and the National Science and Technology Development Agency of Thailand; the Scientific and Technical Research Council of Turkey, and Turkish Atomic Energy Authority; the National Academy of Sciences of Ukraine, and State Fund for Fundamental Researches, Ukraine; the Science and Technology Facilities Council, UK; the US Department of Energy, and the US National Science Foundation.

Individuals have received support from the Marie-Curie program and the European Research Council and EPLANET (European Union); the Leventis Foundation; the A. P. Sloan Foundation; the Alexander von Humboldt Foundation; the Belgian Federal Science Policy Office; the Fonds pour la Formation à la Recherche dans l'Industrie et dans l'Agriculture (FRIA-Belgium); the Agentschap voor Innovatie door Wetenschap en Technologie (IWT-Belgium); the Ministry of Education, Youth and Sports (MEYS) of the Czech Republic; the Council of Science and Industrial Research, India; the HOMING PLUS program of Foundation for Polish Science, cofinanced from European Union, Regional Development Fund; the Compagnia di San Paolo (Torino); the Consorzio per la Fisica (Trieste); MIUR project 20108T4XTM (Italy); the Thalís and Aristeia programs cofinanced by EU-ESF and the Greek NSRF; and the National Priorities Research Program by Qatar National Research Fund.

References

- [1] G. Altarelli, B. Mele, and M. Ruiz-Altaba, "Searching for new heavy vector bosons in $p\bar{p}$ colliders", *Z. Phys. C* **45** (1989) 109, doi:10.1007/BF01556677.
- [2] K. D. Lane, F. E. Paige, T. Skwarnicki, and W. J. Womersley, "Simulations of supercollider physics", *Phys. Rept.* **278** (1997) 291, doi:10.1016/S0370-1573(96)00018-X, arXiv:hep-ph/9412280.
- [3] J. Goodman et al., "Constraints on light Majorana dark matter from colliders", *Phys. Lett. B* **695** (2011) 185, doi:10.1016/j.physletb.2010.11.009, arXiv:1005.1286.
- [4] J. Goodman et al., "Constraints on dark matter from colliders", *Phys. Rev. D* **82** (2010) 116010, doi:10.1103/PhysRevD.82.116010, arXiv:1008.1783.
- [5] M. Beltran, D. Hooper, E. W. Kolb, and Z. A. C. Krusberg, "Deducing the nature of dark matter from direct and indirect detection experiments in the absence of collider signatures of new physics", *Phys. Rev. D* **80** (2009) 043509, doi:10.1103/PhysRevD.80.043509, arXiv:0808.3384.
- [6] E. Accomando et al., "Interference effects in heavy W' -boson searches at the LHC", *Phys. Rev. D* **85** (2012) 115017, doi:10.1103/PhysRevD.85.115017, arXiv:1110.0713.
- [7] T. G. Rizzo, "The determination of the helicity of W' boson couplings at the LHC", *JHEP* **05** (2007) 037, doi:10.1088/1126-6708/2007/05/037.
- [8] E. Boos, V. Bunichev, L. Dudko, and M. Perfilov, "Interference between W' and W in single-top quark production processes", *Phys. Lett. B* **655** (2007) 245, doi:10.1016/j.physletb.2007.03.064, arXiv:hep-ph/0610080.
- [9] C.-R. Chen et al., "Dark matter and collider phenomenology of split-UED", *JHEP* **09** (2009) 078, doi:10.1088/1126-6708/2009/09/078, arXiv:0903.1971.

- [10] K. Kong, S. C. Park, and T. G. Rizzo, “Collider phenomenology with Split-UED”, *JHEP* **04** (2010) 081, doi:10.1007/JHEP04(2010)081, arXiv:1002.0602.
- [11] K. R. Dienes, E. Dudas, and T. Gherghetta, “Grand unification at intermediate mass scales through extra dimensions”, *Nucl. Phys. B* **537** (1999) 47, doi:10.1016/S0550-3213(98)00669-5, arXiv:hep-ph/9806292.
- [12] A. Pomarol and M. Quiros, “The standard model from extra dimensions”, *Phys. Lett. B* **438** (1998) 255, doi:10.1016/S0370-2693(98)00979-4, arXiv:hep-ph/9806263.
- [13] M. Masip and A. Pomarol, “Effects of standard model Kaluza-Klein excitations on electroweak observables”, *Phys. Rev. D* **60** (1999) 096005, doi:10.1103/PhysRevD.60.096005, arXiv:hep-ph/9902467.
- [14] I. Antoniadis, K. Benakli, and M. Quiros, “Direct collider signatures of large extra dimensions”, *Phys. Lett. B* **460** (1999) 176, doi:10.1016/S0370-2693(99)00764-9, arXiv:hep-ph/9905311.
- [15] D0 Collaboration, “Search for W' bosons decaying to an electron and a neutrino with the D0 detector”, *Phys. Rev. Lett.* **100** (2008) 031804, doi:10.1103/PhysRevLett.100.031804, arXiv:0710.2966.
- [16] CDF Collaboration, “Search for a new heavy gauge boson W' with event signature electron + missing transverse energy in $p\bar{p}$ collisions at $\sqrt{s} = 1.96$ TeV”, *Phys. Rev. D* **83** (2011) 031102, doi:10.1103/PhysRevD.83.031102, arXiv:1012.5145.
- [17] ATLAS Collaboration, “Search for high-mass states with one lepton plus missing transverse momentum in proton-proton collisions at $\sqrt{s} = 7$ TeV with the ATLAS detector”, *Phys. Lett. B* **701** (2011) 50, doi:10.1016/j.physletb.2011.05.043, arXiv:1103.1391.
- [18] ATLAS Collaboration, “Search for a heavy gauge boson decaying to a charged lepton and a neutrino in 1 fb^{-1} of pp collisions at $\sqrt{s} = 7$ TeV using the ATLAS detector”, *Phys. Lett. B* **705** (2011) 28, doi:10.1016/j.physletb.2011.09.093, arXiv:1108.1316.
- [19] ATLAS Collaboration, “ATLAS search for a heavy gauge boson decaying to a charged lepton and a neutrino in pp collisions at $\sqrt{s} = 7$ TeV”, *Eur. Phys. J. C* **72** (2012) 2241, doi:10.1140/epjc/s10052-012-2241-5, arXiv:1209.4446.
- [20] ATLAS Collaboration, “Search for new particles in events with one lepton and missing transverse momentum in pp collisions at $\sqrt{s} = 8$ TeV with the ATLAS detector”, *JHEP* **09** (2014) 037, doi:10.1007/JHEP09(2014)037, arXiv:1407.7494.
- [21] CMS Collaboration, “Search for a heavy gauge boson W' in the final state with an electron and large missing transverse energy in pp collisions at $\sqrt{s} = 7$ TeV”, *Phys. Lett. B* **698** (2011) 21, doi:10.1016/j.physletb.2011.02.048, arXiv:1012.5945.
- [22] CMS Collaboration, “Search for a W' boson decaying to a muon and a neutrino in pp collisions at $\sqrt{s} = 7$ TeV”, *Phys. Lett. B* **701** (2011) 160, doi:10.1016/j.physletb.2011.05.048, arXiv:1103.0030.
- [23] CMS Collaboration, “Search for leptonic decays of W' bosons in pp collisions at $\sqrt{s} = 7$ TeV”, *JHEP* **08** (2012) 023, doi:10.1007/JHEP08(2012)023, arXiv:1204.4764.

- [24] CMS Collaboration, “Search for new physics in final states with a lepton and missing transverse energy in pp collisions at the LHC”, *Phys. Rev. D* **87** (2013) 072005, doi:10.1103/PhysRevD.87.072005, arXiv:1302.2812.
- [25] CMS Collaboration, “CMS Luminosity Based on Pixel Cluster Counting - Summer 2013 Update”, CMS Physics Analysis Summary CMS-PAS-LUM-13-001, 2013.
- [26] CMS Collaboration, “The CMS experiment at the CERN LHC”, *JINST* **3** (2008) S08004, doi:10.1088/1748-0221/3/08/S08004.
- [27] CMS Collaboration, “Energy calibration and resolution of the CMS electromagnetic calorimeter in pp collisions at $\sqrt{s} = 7$ TeV”, *JINST* **8** (2013) P09009, doi:10.1088/1748-0221/8/09/P09009, arXiv:1306.2016.
- [28] CMS Collaboration, “Search for heavy narrow dilepton resonances in pp collisions at $\sqrt{s} = 7$ TeV and $\sqrt{s} = 8$ TeV”, *Phys. Lett. B* **720** (2013) 63, doi:10.1016/j.physletb.2013.02.003, arXiv:1212.6175.
- [29] CMS Collaboration, “Performance of CMS muon reconstruction in pp collision events at $\sqrt{s} = 7$ TeV”, *JINST* **7** (2012) P10002, doi:10.1088/1748-0221/7/10/P10002, arXiv:1206.4071.
- [30] GEANT4 Collaboration, “GEANT4—a simulation toolkit”, *Nucl. Instrum. Meth. A* **506** (2003) 250, doi:10.1016/S0168-9002(03)01368-8.
- [31] J. Allison et al., “Geant4 developments and applications”, *IEEE Trans. Nucl. Sci.* **53** (2006) 270, doi:10.1109/TNS.2006.869826.
- [32] D0 Collaboration, “Search for W' Boson Resonances Decaying to a Top Quark and a Bottom Quark”, *Phys. Rev. Lett.* **100** (2008) 211803, doi:10.1103/PhysRevLett.100.211803, arXiv:0803.3256.
- [33] CMS Collaboration, “Search for $W' \rightarrow tb$ decays in the lepton + jets final state in pp collisions at $\sqrt{s} = 8$ TeV”, *JHEP* **05** (2014) 108, doi:10.1007/JHEP05(2014)108, arXiv:1402.2176.
- [34] ATLAS Collaboration, “Search for tb resonances in proton-proton collisions at $\sqrt{s} = 7$ TeV with the ATLAS detector”, *Phys. Rev. Lett.* **109** (2012) 081801, doi:10.1103/PhysRevLett.109.081801, arXiv:1205.1016.
- [35] CMS Collaboration, “Search for charge-asymmetric production of W' bosons in top pair + jet events from pp collisions at $\sqrt{s} = 7$ TeV”, *Phys. Lett. B* **717** (2012) 351, doi:10.1016/j.physletb.2012.09.048, arXiv:1206.3921.
- [36] CMS Collaboration, “Search for a W' boson decaying to a bottom quark and a top quark in pp collisions at $\sqrt{s} = 7$ TeV”, *Phys. Lett. B* **718** (2013) 1229, doi:10.1016/j.physletb.2012.12.008, arXiv:1208.0956.
- [37] ATLAS Collaboration, “Search for $W' \rightarrow tb \rightarrow qqbb$ Decays in pp Collisions at $\sqrt{s} = 8$ TeV with the ATLAS Detector”, (2014). arXiv:1408.0886. Submitted to Eur. Phys. J. C.
- [38] CMS Collaboration, “Search for a W' or Techni- ρ Decaying into WZ in pp Collisions at $\sqrt{s} = 7$ TeV”, *Phys. Rev. Lett.* **109** (2012) 141801, doi:10.1103/PhysRevLett.109.141801, arXiv:1206.0433.

- [39] CMS Collaboration, “Search for new resonances decaying via WZ to leptons in proton-proton collisions at $\sqrt{s} = 8 \text{ TeV}$ ”, *Phys. Lett. B* **740** (2014) 83, doi:10.1016/j.physletb.2014.11.026, arXiv:1407.3476.
- [40] J. C. Pati and A. Salam, “Lepton number as the fourth ‘color’”, *Phys. Rev. D* **10** (1974) 275, doi:10.1103/PhysRevD.10.275. [Erratum: doi:10.1103/PhysRevD.11.703.2].
- [41] R. N. Mohapatra and J. C. Pati, ““Natural” left-right symmetry”, *Phys. Rev. D* **11** (1975) 2558, doi:10.1103/PhysRevD.11.2558.
- [42] G. Senjanović and R. N. Mohapatra, “Exact left-right symmetry and spontaneous violation of parity”, *Phys. Rev. D* **12** (1975) 1502, doi:10.1103/PhysRevD.12.1502.
- [43] G. Senjanović, “Spontaneous breakdown of parity in a class of gauge theories”, *Nucl. Phys. B* **153** (1979) 334, doi:10.1016/0550-3213(79)90604-7.
- [44] P. Minkowski, “ $\mu \rightarrow e\gamma$ at a rate of one out of 10^9 muon decays?”, *Phys. Lett. B* **67** (1977) 421, doi:10.1016/0370-2693(77)90435-X.
- [45] R. N. Mohapatra and G. Senjanović, “Neutrino Mass and Spontaneous Parity Nonconservation”, *Phys. Rev. Lett.* **44** (1980) 912, doi:10.1103/PhysRevLett.44.912.
- [46] R. N. Mohapatra and G. Senjanović, “Neutrino masses and mixings in gauge models with spontaneous parity violation”, *Phys. Rev. D* **23** (1981) 165, doi:10.1103/PhysRevD.23.165.
- [47] T. Sjöstrand, S. Mrenna, and P. Z. Skands, “PYTHIA 6.4 physics and manual”, *JHEP* **05** (2006) 026, doi:10.1088/1126-6708/2006/05/026, arXiv:hep-ph/0603175.
- [48] J. Pumplin et al., “New generation of parton distributions with uncertainties from global QCD analysis”, *JHEP* **07** (2002) 012, doi:10.1088/1126-6708/2002/07/012, arXiv:hep-ph/0201195.
- [49] R. Gavin, Y. Li, F. Petriello, and S. Quackenbush, “FEWZ 2.0: A code for hadronic Z production at next-to-next-to-leading order”, *Comput. Phys. Commun.* **182** (2011) 2388, doi:10.1016/j.cpc.2011.06.008, arXiv:1011.3540.
- [50] R. Gavin, Y. Li, F. Petriello, and S. Quackenbush, “W Physics at the LHC with FEWZ 2.1”, *Comput. Phys. Commun.* **184** (2013) 208, doi:10.1016/j.cpc.2012.09.005, arXiv:1201.5896.
- [51] H. Terazawa, M. Yasue, K. Akama, and M. Hayashi, “Observable effects of the possible substructure of leptons and quarks”, *Phys. Lett. B* **112** (1982) 387, doi:10.1016/0370-2693(82)91075-9.
- [52] CDF Collaboration, “Search for quark lepton compositeness and a heavy W' boson using the $e\nu$ channel in $p\bar{p}$ collisions at $\sqrt{s} = 1.8 \text{ TeV}$ ”, *Phys. Rev. Lett.* **87** (2001) 231803, doi:10.1103/PhysRevLett.87.231803, arXiv:hep-ex/0107008.
- [53] CMS Collaboration, “Search for dark matter, extra dimensions, and unparticles in monojet events in proton-proton collisions at $\sqrt{s} = 8 \text{ TeV}$ ”, (2014). arXiv:1408.3583. Submitted to Eur. Phys. J. C.

- [54] CMS Collaboration, “Search for new phenomena in monophoton final states in proton-proton collisions at $\sqrt{s} = 8$ TeV”, (2014). arXiv:1410.8812. Submitted to Phys. Lett. B.
- [55] Y. Bai and T. M. P. Tait, “Searches with mono-leptons”, *Phys. Lett. B* **723** (2013) 384, doi:10.1016/j.physletb.2013.05.057, arXiv:1208.4361.
- [56] Particle Data Group, J. Beringer et al., “Review of Particle Physics”, *Phys. Rev. D* **86** (2012) 010001, doi:10.1103/PhysRevD.86.010001.
- [57] J. Alwall et al., “MadGraph 5: going beyond”, *JHEP* **06** (2011) 128, doi:10.1007/JHEP06(2011)128, arXiv:1106.0522.
- [58] J. Alwall et al., “MadGraph/MadEvent v4: the new web generation”, *JHEP* **09** (2007) 028, doi:10.1088/1126-6708/2007/09/028.
- [59] R. Field, “Early LHC Underlying Event Data - Findings and Surprises”, in *22nd Hadron Collider Physics Symposium (HCP 2010)*, W. Trischuk, ed. Toronto, 2010. arXiv:1010.3558.
- [60] CMS Collaboration, “Particle-Flow Event Reconstruction in CMS and Performance for Jets, Taus, and E_T^{miss} ”, CMS Physics Analysis Summary CMS-PAS-PFT-09-001, 2009.
- [61] CMS Collaboration, “Commissioning of the Particle-flow Event Reconstruction with the first LHC collisions recorded in the CMS detector”, CMS Physics Analysis Summary CMS-PAS-PFT-10-001, 2010.
- [62] CMS Collaboration, “Commissioning of the Particle-Flow Reconstruction in Minimum-Bias and Jet Events from pp Collisions at 7 TeV”, CMS Physics Analysis Summary CMS-PAS-PFT-10-002, 2010.
- [63] CMS Collaboration, “Determination of jet energy calibration and transverse momentum resolution in CMS”, *JINST* **6** (2011) P11002, doi:10.1088/1748-0221/6/11/P11002, arXiv:1107.4277.
- [64] CMS Collaboration, “Missing transverse energy performance of the CMS detector”, *JINST* **6** (2011) P09001, doi:10.1088/1748-0221/6/09/P09001, arXiv:1106.5048.
- [65] CMS Collaboration, “Measurements of Inclusive W and Z Cross Sections in pp Collisions at $\sqrt{s} = 7$ TeV”, *JHEP* **01** (2011) 080, doi:10.1007/JHEP01(2011)080, arXiv:1012.2466.
- [66] CMS Collaboration, “Single Muon efficiencies in 2012 Data”, CMS Detector Performance Summary CMS-DP-2013-009, 2013.
- [67] F. Garwood, “Fiducial Limits for the Poisson Distribution”, *Biometrika* **28** (1936), no. 3-4, 437, doi:10.1093/biomet/28.3-4.437.
- [68] S. Frixione and B. R. Webber, “Matching NLO QCD computations and parton shower simulations”, *JHEP* **06** (2002) 029, doi:10.1088/1126-6708/2002/06/029, arXiv:hep-ph/0204244.
- [69] S. Frixione, P. Nason, and B. R. Webber, “Matching NLO QCD and parton showers in heavy flavor production”, *JHEP* **08** (2003) 007, doi:10.1088/1126-6708/2003/08/007, arXiv:hep-ph/0305252.

- [70] G. Corcella et al., “HERWIG 6: an event generator for hadron emission reactions with interfering gluons (including supersymmetric processes)”, *JHEP* **01** (2001) 010, doi:10.1088/1126-6708/2001/01/010, arXiv:hep-ph/0011363.
- [71] P. Nason, “A new method for combining NLO QCD with shower Monte Carlo algorithms”, *JHEP* **11** (2004) 040, doi:10.1088/1126-6708/2004/11/040, arXiv:hep-ph/0409146.
- [72] S. Frixione, P. Nason, and C. Oleari, “Matching NLO QCD computations with Parton Shower simulations: the POWHEG method”, *JHEP* **11** (2007) 070, doi:10.1088/1126-6708/2007/11/070, arXiv:0709.2092.
- [73] S. Alioli, P. Nason, C. Oleari, and E. Re, “A general framework for implementing NLO calculations in shower Monte Carlo programs: the POWHEG BOX”, *JHEP* **06** (2010) 043, doi:10.1007/JHEP06(2010)043, arXiv:1002.2581.
- [74] E. Re, “Single-top Wt -channel production matched with parton showers using the POWHEG method”, *Eur. Phys. J. C* **71** (2011) 1547, doi:10.1140/epjc/s10052-011-1547-z, arXiv:1009.2450.
- [75] M. Czakon, P. Fiedler, and A. Mitov, “Total Top-Quark Pair-Production Cross Section at Hadron Colliders Through $O(\alpha_s^4)$ ”, *Phys. Rev. Lett.* **110** (2013) 252004, doi:10.1103/PhysRevLett.110.252004, arXiv:1303.6254.
- [76] S. Alioli, P. Nason, C. Oleari, and E. Re, “Vector boson plus one jet production in POWHEG”, *JHEP* **01** (2011) 095, doi:10.1007/JHEP01(2011)095, arXiv:1009.5594.
- [77] C. M. C. Calame, G. Montagna, O. Nicrosini, and A. Vicini, “Precision electroweak calculation of the production of a high transverse-momentum lepton pair at hadron colliders”, *JHEP* **10** (2007) 109, doi:10.1088/1126-6708/2007/10/109, arXiv:0710.1722.
- [78] H.-L. Lai et al., “New parton distributions for collider physics”, *Phys. Rev. D* **82** (2010) 074024, doi:10.1103/PhysRevD.82.074024, arXiv:1007.2241.
- [79] G. Balossini et al., “Combination of electroweak and QCD corrections to single W production at the Fermilab Tevatron and the CERN LHC”, *JHEP* **01** (2010) 013, doi:10.1007/JHEP01(2010)013, arXiv:0907.0276.
- [80] S. Alekhin et al., “The PDF4LHC Working Group Interim Report”, (2011). arXiv:1101.0536.
- [81] M. Botje et al., “The PDF4LHC Working Group Interim Recommendations”, (2011). arXiv:1101.0538.
- [82] NNPDF Collaboration, “Impact of heavy quark masses on parton distributions and LHC Phenomenology”, *Nucl. Phys. B* **849** (2011) 296, doi:10.1016/j.nuclphysb.2011.03.021, arXiv:1101.1300.
- [83] A. D. Martin, W. J. Stirling, R. S. Thorne, and G. Watt, “Parton distributions for the LHC”, *Eur. Phys. J. C* **63** (2009) 189, doi:10.1140/epjc/s10052-009-1072-5, arXiv:0901.0002.

-
- [84] A. L. Read, "Presentation of search results: the CL_s technique", *J. Phys. G* **28** (2002) 2693, doi:10.1088/0954-3899/28/10/313.
- [85] T. Junk, "Confidence level computation for combining searches with small statistics", *Nucl. Instrum. Meth. A* **434** (1999) 435, doi:10.1016/S0168-9002(99)00498-2, arXiv:hep-ex/9902006.
- [86] Y. Bai, P. J. Fox, and R. Harnik, "The Tevatron at the frontier of dark matter direct detection", *JHEP* **12** (2010) 048, doi:10.1007/JHEP12(2010)048, arXiv:1005.3797.
- [87] O. Buchmueller, M. J. Dolan, and C. McCabe, "Beyond effective field theory for dark matter searches at the LHC", *JHEP* **01** (2014) 025, doi:10.1007/JHEP01(2014)025, arXiv:1308.6799.
- [88] K.-M. Cheung and G. L. Landsberg, "Kaluza-Klein states of the standard model gauge bosons: constraints from high energy experiments", *Phys. Rev. D* **65** (2002) 076003, doi:10.1103/PhysRevD.65.076003, arXiv:hep-ph/0110346.

A The CMS Collaboration

Yerevan Physics Institute, Yerevan, Armenia

V. Khachatryan, A.M. Sirunyan, A. Tumasyan

Institut für Hochenergiephysik der OeAW, Wien, Austria

W. Adam, T. Bergauer, M. Dragicevic, J. Erö, C. Fabjan¹, M. Friedl, R. Frühwirth¹, V.M. Ghete, C. Hartl, N. Hörmann, J. Hrubec, M. Jeitler¹, W. Kiesenhofer, V. Knünz, M. Krammer¹, I. Krätschmer, D. Liko, I. Mikulec, D. Rabady², B. Rahbaran, H. Rohringer, R. Schöfbeck, J. Strauss, A. Taurok, W. Treberer-Treberspurg, W. Waltenberger, C.-E. Wulz¹

National Centre for Particle and High Energy Physics, Minsk, Belarus

V. Mossolov, N. Shumeiko, J. Suarez Gonzalez

Universiteit Antwerpen, Antwerpen, Belgium

S. Alderweireldt, M. Bansal, S. Bansal, T. Cornelis, E.A. De Wolf, X. Janssen, A. Knutsson, S. Luyckx, S. Ochesanu, B. Roland, R. Rougny, M. Van De Klundert, H. Van Haevermaet, P. Van Mechelen, N. Van Remortel, A. Van Spilbeeck

Vrije Universiteit Brussel, Brussel, Belgium

F. Blekman, S. Blyweert, J. D'Hondt, N. Daci, N. Heracleous, A. Kalogeropoulos, J. Keaveney, T.J. Kim, S. Lowette, M. Maes, A. Olbrechts, Q. Python, D. Strom, S. Tavernier, W. Van Doninck, P. Van Mulders, G.P. Van Onsem, I. Vilella

Université Libre de Bruxelles, Bruxelles, Belgium

C. Caillol, B. Clerbaux, G. De Lentdecker, D. Dobur, L. Favart, A.P.R. Gay, A. Grebenyuk, A. Léonard, A. Mohammadi, L. Perniè², T. Reis, T. Seva, L. Thomas, C. Vander Velde, P. Vanlaer, J. Wang

Ghent University, Ghent, Belgium

V. Adler, K. Beernaert, L. Benucci, A. Cimmino, S. Costantini, S. Crucy, S. Dildick, A. Fagot, G. Garcia, J. Mccartin, A.A. Ocampo Rios, D. Ryckbosch, S. Salva Diblen, M. Sigamani, N. Strobbe, F. Thyssen, M. Tytgat, E. Yazgan, N. Zaganidis

Université Catholique de Louvain, Louvain-la-Neuve, Belgium

S. Basegmez, C. Beluffi³, G. Bruno, R. Castello, A. Caudron, L. Ceard, G.G. Da Silveira, C. Delaere, T. du Pree, D. Favart, L. Forthomme, A. Giammanco⁴, J. Hollar, P. Jez, M. Komm, V. Lemaître, J. Liao, C. Nuttens, D. Pagano, L. Perrini, A. Pin, K. Piotrkowski, A. Popov⁵, L. Quertenmont, M. Selvaggi, M. Vidal Marono, J.M. Vizan Garcia

Université de Mons, Mons, Belgium

N. Bely, T. Caebergs, E. Daubie, G.H. Hammad

Centro Brasileiro de Pesquisas Físicas, Rio de Janeiro, Brazil

W.L. Aldá Júnior, G.A. Alves, M. Correa Martins Junior, T. Dos Reis Martins, M.E. Pol

Universidade do Estado do Rio de Janeiro, Rio de Janeiro, Brazil

W. Carvalho, J. Chinellato⁶, A. Custódio, E.M. Da Costa, D. De Jesus Damiao, C. De Oliveira Martins, S. Fonseca De Souza, H. Malbouisson, M. Malek, D. Matos Figueiredo, L. Mundim, H. Nogima, W.L. Prado Da Silva, J. Santaolalla, A. Santoro, A. Sznajder, E.J. Tonelli Manganote⁶, A. Vilela Pereira

Universidade Estadual Paulista ^a, Universidade Federal do ABC ^b, São Paulo, Brazil

C.A. Bernardes^b, F.A. Dias^{a,7}, T.R. Fernandez Perez Tomei^a, E.M. Gregores^b, P.G. Mercadante^b, S.F. Novaes^a, Sandra S. Padula^a

Institute for Nuclear Research and Nuclear Energy, Sofia, Bulgaria

A. Aleksandrov, V. Genchev², P. Iaydjiev, A. Marinov, S. Piperov, M. Rodozov, G. Sultanov, M. Vutova

University of Sofia, Sofia, Bulgaria

A. Dimitrov, I. Glushkov, R. Hadjiiska, V. Kozhuharov, L. Litov, B. Pavlov, P. Petkov

Institute of High Energy Physics, Beijing, China

J.G. Bian, G.M. Chen, H.S. Chen, M. Chen, R. Du, C.H. Jiang, D. Liang, S. Liang, R. Plestina⁸, J. Tao, X. Wang, Z. Wang

State Key Laboratory of Nuclear Physics and Technology, Peking University, Beijing, China

C. Asawatangtrakuldee, Y. Ban, Y. Guo, Q. Li, W. Li, S. Liu, Y. Mao, S.J. Qian, D. Wang, L. Zhang, W. Zou

Universidad de Los Andes, Bogota, Colombia

C. Avila, L.F. Chaparro Sierra, C. Florez, J.P. Gomez, B. Gomez Moreno, J.C. Sanabria

University of Split, Faculty of Electrical Engineering, Mechanical Engineering and Naval Architecture, Split, Croatia

N. Godinovic, D. Lelas, D. Polic, I. Puljak

University of Split, Faculty of Science, Split, Croatia

Z. Antunovic, M. Kovac

Institute Rudjer Boskovic, Zagreb, Croatia

V. Brigljevic, K. Kadija, J. Luetic, D. Mekterovic, L. Sudic

University of Cyprus, Nicosia, Cyprus

A. Attikis, G. Mavromanolakis, J. Mousa, C. Nicolaou, F. Ptochos, P.A. Razis

Charles University, Prague, Czech Republic

M. Bodlak, M. Finger, M. Finger Jr.⁹

Academy of Scientific Research and Technology of the Arab Republic of Egypt, Egyptian Network of High Energy Physics, Cairo, Egypt

Y. Assran¹⁰, S. Elgammal¹¹, M.A. Mahmoud¹², A. Radi^{11,13}

National Institute of Chemical Physics and Biophysics, Tallinn, Estonia

M. Kadastik, M. Murumaa, M. Raidal, A. Tiko

Department of Physics, University of Helsinki, Helsinki, Finland

P. Eerola, G. Fedi, M. Voutilainen

Helsinki Institute of Physics, Helsinki, Finland

J. Härkönen, V. Karimäki, R. Kinnunen, M.J. Kortelainen, T. Lampén, K. Lassila-Perini, S. Lehti, T. Lindén, P. Luukka, T. Mäenpää, T. Peltola, E. Tuominen, J. Tuominiemi, E. Tuovinen, L. Wendland

Lappeenranta University of Technology, Lappeenranta, Finland

T. Tuuva

DSM/IRFU, CEA/Saclay, Gif-sur-Yvette, France

M. Besancon, F. Couderc, M. Dejardin, D. Denegri, B. Fabbro, J.L. Faure, C. Favaro, F. Ferri, S. Ganjour, A. Givernaud, P. Gras, G. Hamel de Monchenault, P. Jarry, E. Locci, J. Malcles, J. Rander, A. Rosowsky, M. Titov

Laboratoire Leprince-Ringuet, Ecole Polytechnique, IN2P3-CNRS, Palaiseau, France

S. Baffioni, F. Beaudette, P. Busson, C. Charlot, T. Dahms, M. Dalchenko, L. Dobrzynski, N. Filipovic, A. Florent, R. Granier de Cassagnac, L. Mastrolorenzo, P. Miné, C. Mironov, I.N. Naranjo, M. Nguyen, C. Ochando, P. Paganini, R. Salerno, J.B. Sauvan, Y. Sirois, C. Veelken, Y. Yilmaz, A. Zabi

Institut Pluridisciplinaire Hubert Curien, Université de Strasbourg, Université de Haute Alsace Mulhouse, CNRS/IN2P3, Strasbourg, France

J.-L. Agram¹⁴, J. Andrea, A. Aubin, D. Bloch, J.-M. Brom, E.C. Chabert, C. Collard, E. Conte¹⁴, J.-C. Fontaine¹⁴, D. Gelé, U. Goerlach, C. Goetzmann, A.-C. Le Bihan, P. Van Hove

Centre de Calcul de l'Institut National de Physique Nucleaire et de Physique des Particules, CNRS/IN2P3, Villeurbanne, France

S. Gadrat

Université de Lyon, Université Claude Bernard Lyon 1, CNRS-IN2P3, Institut de Physique Nucléaire de Lyon, Villeurbanne, France

S. Beauceron, N. Beaupere, G. Boudoul², S. Brochet, C.A. Carrillo Montoya, J. Chasserat, R. Chierici, D. Contardo², P. Depasse, H. El Mamouni, J. Fan, J. Fay, S. Gascon, M. Gouzevitch, B. Ille, T. Kurca, M. Lethuillier, L. Mirabito, S. Perries, J.D. Ruiz Alvarez, D. Sabes, L. Sgandurra, V. Sordini, M. Vander Donckt, P. Verdier, S. Viret, H. Xiao

Institute of High Energy Physics and Informatization, Tbilisi State University, Tbilisi, Georgia

Z. Tsamalaidze⁹

RWTH Aachen University, I. Physikalisches Institut, Aachen, Germany

C. Autermann, S. Beranek, M. Bontenackels, M. Edelhoff, L. Feld, O. Hindrichs, K. Klein, A. Ostapchuk, A. Perieanu, F. Raupach, J. Sammet, S. Schael, H. Weber, B. Wittmer, V. Zhukov⁵

RWTH Aachen University, III. Physikalisches Institut A, Aachen, Germany

M. Ata, E. Dietz-Laursonn, D. Duchardt, M. Erdmann, S. Erdweg, R. Fischer, A. Güth, T. Hebbeker, C. Heidemann, K. Hoepfner, D. Klingebiel, S. Knutzen, P. Kreuzer, M. Merschmeyer, A. Meyer, P. Millet, M. Olschewski, K. Padeken, P. Papacz, H. Reithler, S.A. Schmitz, L. Sonnenschein, D. Teysier, S. Thüer, M. Weber

RWTH Aachen University, III. Physikalisches Institut B, Aachen, Germany

V. Cherepanov, Y. Erdogan, G. Flügge, H. Geenen, M. Geisler, W. Haj Ahmad, F. Hoehle, B. Kargoll, T. Kress, Y. Kuessel, J. Lingemann², A. Nowack, I.M. Nugent, L. Perchalla, O. Pooth, A. Stahl

Deutsches Elektronen-Synchrotron, Hamburg, Germany

I. Asin, N. Bartosik, J. Behr, W. Behrenhoff, U. Behrens, A.J. Bell, M. Bergholz¹⁵, A. Bethani, K. Borras, A. Burgmeier, A. Cakir, L. Calligaris, A. Campbell, S. Choudhury, F. Costanza, C. Diez Pardos, S. Dooling, T. Dorland, G. Eckerlin, D. Eckstein, T. Eichhorn, G. Flucke, J. Garay Garcia, A. Geiser, P. Gunnellini, J. Hauk, G. Hellwig, M. Hempel, D. Horton, H. Jung, M. Kasemann, P. Katsas, J. Kieseler, C. Kleinwort, D. Krücker, W. Lange, J. Leonard, K. Lipka, A. Lobanov, W. Lohmann¹⁵, B. Lutz, R. Mankel, I. Marfin, I.-A. Melzer-Pellmann, A.B. Meyer, J. Mnich, A. Mussgiller, S. Naumann-Emme, A. Nayak, O. Novgorodova, F. Nowak, E. Ntomari, H. Perrey, D. Pitzl, R. Placakyte, A. Raspereza, P.M. Ribeiro Cipriano, E. Ron, M.Ö. Sahin, J. Salfeld-Nebgen, P. Saxena, R. Schmidt¹⁵, T. Schoerner-Sadenius, M. Schröder, S. Spannagel, A.D.R. Vargas Trevino, R. Walsh, C. Wissing

University of Hamburg, Hamburg, Germany

M. Aldaya Martin, V. Blobel, M. Centis Vignali, J. Erfle, E. Garutti, K. Goebel, M. Görner, J. Haller, M. Hoffmann, R.S. Höing, H. Kirschenmann, R. Klanner, R. Kogler, J. Lange, T. Lapsien, T. Lenz, I. Marchesini, J. Ott, T. Peiffer, N. Pietsch, D. Rathjens, C. Sander, H. Schettler, P. Schleper, E. Schlieckau, A. Schmidt, M. Seidel, J. Sibille¹⁶, V. Sola, H. Stadie, G. Steinbrück, D. Troendle, E. Usai, L. Vanelderen

Institut für Experimentelle Kernphysik, Karlsruhe, Germany

C. Barth, C. Baus, J. Berger, C. Böser, E. Butz, T. Chwalek, W. De Boer, A. Descroix, A. Dierlamm, M. Feindt, F. Frensch, M. Giffels, F. Hartmann², T. Hauth², U. Husemann, I. Katkov⁵, A. Kornmayer², E. Kuznetsova, P. Lobelle Pardo, M.U. Mozer, Th. Müller, A. Nürnberg, G. Quast, K. Rabbertz, F. Ratnikov, S. Röcker, H.J. Simonis, F.M. Stober, R. Ulrich, J. Wagner-Kuhr, S. Wayand, T. Weiler, R. Wolf

Institute of Nuclear and Particle Physics (INPP), NCSR Demokritos, Aghia Paraskevi, Greece

G. Anagnostou, G. Daskalakis, T. Gerasis, V.A. Giakoumopoulou, A. Kyriakis, D. Loukas, A. Markou, C. Markou, A. Psallidas, I. Topsis-Giotis

University of Athens, Athens, Greece

A. Panagiotou, N. Saoulidou, E. Stiliaris

University of Ioánnina, Ioánnina, Greece

X. Aslanoglou, I. Evangelou, G. Flouris, C. Foudas, P. Kokkas, N. Manthos, I. Papadopoulos, E. Paradas

Wigner Research Centre for Physics, Budapest, Hungary

G. Bencze, C. Hajdu, P. Hidas, D. Horvath¹⁷, F. Sikler, V. Veszpremi, G. Vesztergombi¹⁸, A.J. Zsigmond

Institute of Nuclear Research ATOMKI, Debrecen, Hungary

N. Beni, S. Czellar, J. Karancsi¹⁹, J. Molnar, J. Palinkas, Z. Szillasi

University of Debrecen, Debrecen, Hungary

P. Raics, Z.L. Trocsanyi, B. Ujvari

National Institute of Science Education and Research, Bhubaneswar, India

S.K. Swain

Panjab University, Chandigarh, India

S.B. Beri, V. Bhatnagar, N. Dhingra, R. Gupta, U. Bhawandeep, A.K. Kalsi, M. Kaur, M. Mittal, N. Nishu, J.B. Singh

University of Delhi, Delhi, India

Ashok Kumar, Arun Kumar, S. Ahuja, A. Bhardwaj, B.C. Choudhary, A. Kumar, S. Malhotra, M. Naimuddin, K. Ranjan, V. Sharma

Saha Institute of Nuclear Physics, Kolkata, India

S. Banerjee, S. Bhattacharya, K. Chatterjee, S. Dutta, B. Gomber, Sa. Jain, Sh. Jain, R. Khurana, A. Modak, S. Mukherjee, D. Roy, S. Sarkar, M. Sharan

Bhabha Atomic Research Centre, Mumbai, India

A. Abdulsalam, D. Dutta, S. Kailas, V. Kumar, A.K. Mohanty², L.M. Pant, P. Shukla, A. Topkar

Tata Institute of Fundamental Research, Mumbai, India

T. Aziz, S. Banerjee, R.M. Chatterjee, R.K. Dewanjee, S. Dugad, S. Ganguly, S. Ghosh,

M. Guchait, A. Gurtu²⁰, G. Kole, S. Kumar, M. Maity²¹, G. Majumder, K. Mazumdar, G.B. Mohanty, B. Parida, K. Sudhakar, N. Wickramage²²

Institute for Research in Fundamental Sciences (IPM), Tehran, Iran

H. Bakhshiansohi, H. Behnamian, S.M. Etesami²³, A. Fahim²⁴, R. Goldouzian, A. Jafari, M. Khakzad, M. Mohammadi Najafabadi, M. Naseri, S. Paktinat Mehdiabadi, B. Safarzadeh²⁵, M. Zeinali

University College Dublin, Dublin, Ireland

M. Felcini, M. Grunewald

INFN Sezione di Bari ^a, Università di Bari ^b, Politecnico di Bari ^c, Bari, Italy

M. Abbrescia^{a,b}, L. Barbone^{a,b}, C. Calabria^{a,b}, S.S. Chhibra^{a,b}, A. Colaleo^a, D. Creanza^{a,c}, N. De Filippis^{a,c}, M. De Palma^{a,b}, L. Fiore^a, G. Iaselli^{a,c}, G. Maggi^{a,c}, M. Maggi^a, S. My^{a,c}, S. Nuzzo^{a,b}, A. Pompili^{a,b}, G. Pugliese^{a,c}, R. Radogna^{a,b,2}, G. Selvaggi^{a,b}, L. Silvestris^{a,2}, G. Singh^{a,b}, R. Venditti^{a,b}, P. Verwilligen^a, G. Zito^a

INFN Sezione di Bologna ^a, Università di Bologna ^b, Bologna, Italy

G. Abbiendi^a, A.C. Benvenuti^a, D. Bonacorsi^{a,b}, S. Braibant-Giacomelli^{a,b}, L. Brigliadori^{a,b}, R. Campanini^{a,b}, P. Capiluppi^{a,b}, A. Castro^{a,b}, F.R. Cavallo^a, G. Codispoti^{a,b}, M. Cuffiani^{a,b}, G.M. Dallavalle^a, F. Fabbri^a, A. Fanfani^{a,b}, D. Fasanella^{a,b}, P. Giacomelli^a, C. Grandi^a, L. Guiducci^{a,b}, S. Marcellini^a, G. Masetti^{a,2}, A. Montanari^a, F.L. Navarria^{a,b}, A. Perrotta^a, F. Primavera^{a,b}, A.M. Rossi^{a,b}, T. Rovelli^{a,b}, G.P. Siroli^{a,b}, N. Tosi^{a,b}, R. Travaglini^{a,b}

INFN Sezione di Catania ^a, Università di Catania ^b, CSFNSM ^c, Catania, Italy

S. Albergo^{a,b}, G. Cappello^a, M. Chiorboli^{a,b}, S. Costa^{a,b}, F. Giordano^{a,c,2}, R. Potenza^{a,b}, A. Tricomi^{a,b}, C. Tuve^{a,b}

INFN Sezione di Firenze ^a, Università di Firenze ^b, Firenze, Italy

G. Barbagli^a, V. Ciulli^{a,b}, C. Civinini^a, R. D'Alessandro^{a,b}, E. Focardi^{a,b}, E. Gallo^a, S. Gonzi^{a,b}, V. Gori^{a,b,2}, P. Lenzi^{a,b}, M. Meschini^a, S. Paoletti^a, G. Sguazzoni^a, A. Tropiano^{a,b}

INFN Laboratori Nazionali di Frascati, Frascati, Italy

L. Benussi, S. Bianco, F. Fabbri, D. Piccolo

INFN Sezione di Genova ^a, Università di Genova ^b, Genova, Italy

F. Ferro^a, M. Lo Vetere^{a,b}, E. Robutti^a, S. Tosi^{a,b}

INFN Sezione di Milano-Bicocca ^a, Università di Milano-Bicocca ^b, Milano, Italy

M.E. Dinardo^{a,b}, S. Fiorendi^{a,b,2}, S. Gennai^{a,2}, R. Gerosa², A. Ghezzi^{a,b}, P. Govoni^{a,b}, M.T. Lucchini^{a,b,2}, S. Malvezzi^a, R.A. Manzoni^{a,b}, A. Martelli^{a,b}, B. Marzocchi, D. Menasce^a, L. Moroni^a, M. Paganoni^{a,b}, D. Pedrini^a, S. Ragazzi^{a,b}, N. Redaelli^a, T. Tabarelli de Fatis^{a,b}

INFN Sezione di Napoli ^a, Università di Napoli 'Federico II' ^b, Università della Basilicata (Potenza) ^c, Università G. Marconi (Roma) ^d, Napoli, Italy

S. Buontempo^a, N. Cavallo^{a,c}, S. Di Guida^{a,d,2}, F. Fabozzi^{a,c}, A.O.M. Iorio^{a,b}, L. Lista^a, S. Meola^{a,d,2}, M. Merola^a, P. Paolucci^{a,2}

INFN Sezione di Padova ^a, Università di Padova ^b, Università di Trento (Trento) ^c, Padova, Italy

P. Azzi^a, N. Bacchetta^a, D. Bisello^{a,b}, A. Branca^{a,b}, R. Carlin^{a,b}, P. Checchia^a, M. Dall'Osso^{a,b}, T. Dorigo^a, S. Fantinel^a, M. Galanti^{a,b}, F. Gasparini^{a,b}, U. Gasparini^{a,b}, P. Giubilato^{a,b}, A. Gozzelino^a, K. Kanishchev^{a,c}, S. Lacaprara^a, M. Margoni^{a,b}, A.T. Meneguzzo^{a,b}, J. Pazzini^{a,b}, N. Pozzobon^{a,b}, P. Ronchese^{a,b}, F. Simonetto^{a,b}, E. Torassa^a, M. Tosi^{a,b}, P. Zotto^{a,b}, A. Zucchetta^{a,b}, G. Zumerle^{a,b}

INFN Sezione di Pavia ^a, Università di Pavia ^b, Pavia, ItalyM. Gabusi^{a,b}, S.P. Ratti^{a,b}, C. Riccardi^{a,b}, P. Salvini^a, P. Vitulo^{a,b}**INFN Sezione di Perugia ^a, Università di Perugia ^b, Perugia, Italy**M. Biasini^{a,b}, G.M. Bilei^a, D. Ciangottini^{a,b}, L. Fanò^{a,b}, P. Lariccia^{a,b}, G. Mantovani^{a,b}, M. Menichelli^a, F. Romeo^{a,b}, A. Saha^a, A. Santocchia^{a,b}, A. Spiezia^{a,b,2}**INFN Sezione di Pisa ^a, Università di Pisa ^b, Scuola Normale Superiore di Pisa ^c, Pisa, Italy**K. Androsov^{a,26}, P. Azzurri^a, G. Bagliesi^a, J. Bernardini^a, T. Boccali^a, G. Broccolo^{a,c}, R. Castaldi^a, M.A. Ciocci^{a,26}, R. Dell'Orso^a, S. Donato^{a,c}, F. Fiori^{a,c}, L. Foà^{a,c}, A. Giassi^a, M.T. Grippo^{a,26}, F. Ligabue^{a,c}, T. Lomtadze^a, L. Martini^{a,b}, A. Messineo^{a,b}, C.S. Moon^{a,27}, F. Palla^{a,2}, A. Rizzi^{a,b}, A. Savoy-Navarro^{a,28}, A.T. Serban^a, P. Spagnolo^a, P. Squillacioti^{a,26}, R. Tenchini^a, G. Tonelli^{a,b}, A. Venturi^a, P.G. Verdini^a, C. Vernieri^{a,c,2}**INFN Sezione di Roma ^a, Università di Roma ^b, Roma, Italy**L. Barone^{a,b}, F. Cavallari^a, D. Del Re^{a,b}, M. Diemoz^a, M. Grassi^{a,b}, C. Jorda^a, E. Longo^{a,b}, F. Margaroli^{a,b}, P. Meridiani^a, F. Micheli^{a,b,2}, S. Nourbakhsh^{a,b}, G. Organtini^{a,b}, R. Paramatti^a, S. Rahatlou^{a,b}, C. Rovelli^a, F. Santanastasio^{a,b}, L. Soffi^{a,b,2}, P. Traczyk^{a,b}**INFN Sezione di Torino ^a, Università di Torino ^b, Università del Piemonte Orientale (Novara) ^c, Torino, Italy**N. Amapane^{a,b}, R. Arcidiacono^{a,c}, S. Argiro^{a,b,2}, M. Arneodo^{a,c}, R. Bellan^{a,b}, C. Biino^a, N. Cartiglia^a, S. Casasso^{a,b,2}, M. Costa^{a,b}, A. Degano^{a,b}, N. Demaria^a, L. Finco^{a,b}, C. Mariotti^a, S. Maselli^a, E. Migliore^{a,b}, V. Monaco^{a,b}, M. Musich^a, M.M. Obertino^{a,c,2}, G. Ortona^{a,b}, L. Pacher^{a,b}, N. Pastrone^a, M. Pelliccioni^a, G.L. Pinna Angioni^{a,b}, A. Potenza^{a,b}, A. Romero^{a,b}, M. Ruspa^{a,c}, R. Sacchi^{a,b}, A. Solano^{a,b}, A. Staiano^a, U. Tamponi^a**INFN Sezione di Trieste ^a, Università di Trieste ^b, Trieste, Italy**S. Belforte^a, V. Candelise^{a,b}, M. Casarsa^a, F. Cossutti^a, G. Della Ricca^{a,b}, B. Gobbo^a, C. La Licata^{a,b}, M. Marone^{a,b}, D. Montanino^{a,b}, A. Schizzi^{a,b,2}, T. Umer^{a,b}, A. Zanetti^a**Kangwon National University, Chunchon, Korea**

S. Chang, A. Kropivnitskaya, S.K. Nam

Kyungpook National University, Daegu, Korea

D.H. Kim, G.N. Kim, M.S. Kim, D.J. Kong, S. Lee, Y.D. Oh, H. Park, A. Sakharov, D.C. Son

Chonnam National University, Institute for Universe and Elementary Particles, Kwangju, Korea

J.Y. Kim, S. Song

Korea University, Seoul, Korea

S. Choi, D. Gyun, B. Hong, M. Jo, H. Kim, Y. Kim, B. Lee, K.S. Lee, S.K. Park, Y. Roh

University of Seoul, Seoul, Korea

M. Choi, J.H. Kim, I.C. Park, S. Park, G. Ryu, M.S. Ryu

Sungkyunkwan University, Suwon, Korea

Y. Choi, Y.K. Choi, J. Goh, E. Kwon, J. Lee, H. Seo, I. Yu

Vilnius University, Vilnius, Lithuania

A. Juodagalvis

National Centre for Particle Physics, Universiti Malaya, Kuala Lumpur, Malaysia

J.R. Komaragiri

Centro de Investigacion y de Estudios Avanzados del IPN, Mexico City, Mexico

H. Castilla-Valdez, E. De La Cruz-Burelo, I. Heredia-de La Cruz²⁹, R. Lopez-Fernandez, A. Sanchez-Hernandez

Universidad Iberoamericana, Mexico City, Mexico

S. Carrillo Moreno, F. Vazquez Valencia

Benemerita Universidad Autonoma de Puebla, Puebla, Mexico

I. Pedraza, H.A. Salazar Ibarguen

Universidad Autónoma de San Luis Potosí, San Luis Potosí, Mexico

E. Casimiro Linares, A. Morelos Pineda

University of Auckland, Auckland, New Zealand

D. Krofcheck

University of Canterbury, Christchurch, New Zealand

P.H. Butler, S. Reucroft

National Centre for Physics, Quaid-I-Azam University, Islamabad, Pakistan

A. Ahmad, M. Ahmad, Q. Hassan, H.R. Hoorani, S. Khalid, W.A. Khan, T. Khurshid, M.A. Shah, M. Shoaib

National Centre for Nuclear Research, Swierk, Poland

H. Bialkowska, M. Bluj, B. Boimska, T. Frueboes, M. Górski, M. Kazana, K. Nawrocki, K. Romanowska-Rybinska, M. Szleper, P. Zalewski

Institute of Experimental Physics, Faculty of Physics, University of Warsaw, Warsaw, Poland

G. Brona, K. Bunkowski, M. Cwiok, W. Dominik, K. Doroba, A. Kalinowski, M. Konecki, J. Krolikowski, M. Misiura, M. Olszewski, W. Wolszczak

Laboratório de Instrumentação e Física Experimental de Partículas, Lisboa, Portugal

P. Bargassa, C. Beirão Da Cruz E Silva, P. Faccioli, P.G. Ferreira Parracho, M. Gallinaro, F. Nguyen, J. Rodrigues Antunes, J. Seixas, J. Varela, P. Vischia

Joint Institute for Nuclear Research, Dubna, Russia

P. Bunin, M. Gavrilenko, I. Golutvin, A. Kamenev, V. Karjavin, V. Konoplyanikov, A. Lanev, A. Malakhov, V. Matveev³⁰, P. Moisezenz, V. Palichik, V. Perelygin, M. Savina, S. Shmatov, S. Shulha, N. Skatchkov, V. Smirnov, A. Zarubin

Petersburg Nuclear Physics Institute, Gatchina (St. Petersburg), Russia

V. Golovtsov, Y. Ivanov, V. Kim³¹, P. Levchenko, V. Murzin, V. Oreshkin, I. Smirnov, V. Sulimov, L. Uvarov, S. Vavilov, A. Vorobyev, An. Vorobyev

Institute for Nuclear Research, Moscow, Russia

Yu. Andreev, A. Dermenev, S. Gninenko, N. Golubev, M. Kirsanov, N. Krasnikov, A. Pashenkov, D. Tlisov, A. Toropin

Institute for Theoretical and Experimental Physics, Moscow, Russia

V. Epshteyn, V. Gavrilov, N. Lychkovskaya, V. Popov, G. Safronov, S. Semenov, A. Spiridonov, V. Stolin, E. Vlasov, A. Zhokin

P.N. Lebedev Physical Institute, Moscow, Russia

V. Andreev, M. Azarkin, I. Dremin, M. Kirakosyan, A. Leonidov, G. Mesyats, S.V. Rusakov, A. Vinogradov

Skobeltsyn Institute of Nuclear Physics, Lomonosov Moscow State University, Moscow, Russia

A. Belyaev, E. Boos, V. Bunichev, M. Dubinin⁷, L. Dudko, A. Ershov, A. Gribushin, V. Klyukhin, O. Kodolova, I. Lokhtin, S. Obraztsov, M. Perfilov, V. Savrin

State Research Center of Russian Federation, Institute for High Energy Physics, Protvino, Russia

I. Azhgirey, I. Bayshev, S. Bitioukov, V. Kachanov, A. Kalinin, D. Konstantinov, V. Krychkin, V. Petrov, R. Ryutin, A. Sobol, L. Tourtchanovitch, S. Troshin, N. Tyurin, A. Uzunian, A. Volkov

University of Belgrade, Faculty of Physics and Vinca Institute of Nuclear Sciences, Belgrade, Serbia

P. Adzic³², M. Dordevic, M. Ekmedzic, J. Milosevic

Centro de Investigaciones Energéticas Medioambientales y Tecnológicas (CIEMAT), Madrid, Spain

J. Alcaraz Maestre, C. Battilana, E. Calvo, M. Cerrada, M. Chamizo Llatas², N. Colino, B. De La Cruz, A. Delgado Peris, D. Domínguez Vázquez, A. Escalante Del Valle, C. Fernandez Bedoya, J.P. Fernández Ramos, J. Flix, M.C. Fouz, P. Garcia-Abia, O. Gonzalez Lopez, S. Goy Lopez, J.M. Hernandez, M.I. Josa, G. Merino, E. Navarro De Martino, A. Pérez-Calero Yzquierdo, J. Puerta Pelayo, A. Quintario Olmeda, I. Redondo, L. Romero, M.S. Soares

Universidad Autónoma de Madrid, Madrid, Spain

C. Albajar, J.F. de Trocóniz, M. Missiroli

Universidad de Oviedo, Oviedo, Spain

H. Brun, J. Cuevas, J. Fernandez Menendez, S. Folgueras, I. Gonzalez Caballero, L. Lloret Iglesias

Instituto de Física de Cantabria (IFCA), CSIC-Universidad de Cantabria, Santander, Spain

J.A. Brochero Cifuentes, I.J. Cabrillo, A. Calderon, J. Duarte Campderros, M. Fernandez, G. Gomez, A. Graziano, A. Lopez Virto, J. Marco, R. Marco, C. Martinez Rivero, F. Matorras, F.J. Munoz Sanchez, J. Piedra Gomez, T. Rodrigo, A.Y. Rodríguez-Marrero, A. Ruiz-Jimeno, L. Scodellaro, I. Vila, R. Vilar Cortabitarte

CERN, European Organization for Nuclear Research, Geneva, Switzerland

D. Abbaneo, E. Auffray, G. Auzinger, M. Bachtis, P. Baillon, A.H. Ball, D. Barney, A. Benaglia, J. Bendavid, L. Benhabib, J.F. Benitez, C. Bernet⁸, G. Bianchi, P. Bloch, A. Bocci, A. Bonato, O. Bondu, C. Botta, H. Breuker, T. Camporesi, G. Cerminara, S. Colafranceschi³³, M. D'Alfonso, D. d'Enterria, A. Dabrowski, A. David, F. De Guio, A. De Roeck, S. De Visscher, M. Dobson, N. Dupont-Sagorin, A. Elliott-Peisert, J. Eugster, G. Franzoni, W. Funk, D. Gigi, K. Gill, D. Giordano, M. Girone, F. Glege, R. Guida, S. Gundacker, M. Guthoff, J. Hammer, M. Hansen, P. Harris, J. Hegeman, V. Innocente, P. Janot, K. Kousouris, K. Krajczar, P. Lecoq, C. Lourenço, N. Magini, L. Malgeri, M. Mannelli, J. Marrouche, L. Masetti, F. Meijers, S. Mersi, E. Meschi, F. Moortgat, S. Morovic, M. Mulders, P. Musella, L. Orsini, L. Pape, E. Perez, L. Perrozzi, A. Petrilli, G. Petrucciani, A. Pfeiffer, M. Pierini, M. Pimiä, D. Piparo, M. Plagge, A. Racz, G. Rolandi³⁴, M. Rovere, H. Sakulin, C. Schäfer, C. Schwick, S. Sekmen, A. Sharma, P. Siegrist, P. Silva, M. Simon, P. Sphicas³⁵, D. Spiga, J. Steggemann, B. Stieger, M. Stoye, D. Treille, A. Tsiros, G.I. Veres¹⁸, J.R. Vlimant, N. Wardle, H.K. Wöhri, W.D. Zeuner

Paul Scherrer Institut, Villigen, Switzerland

W. Bertl, K. Deiters, W. Erdmann, R. Horisberger, Q. Ingram, H.C. Kaestli, S. König, D. Kotlinski, U. Langenegger, D. Renker, T. Rohe

Institute for Particle Physics, ETH Zurich, Zurich, Switzerland

F. Bachmair, L. Bäni, L. Bianchini, P. Bortignon, M.A. Buchmann, B. Casal, N. Chanon, A. Deisher, G. Dissertori, M. Dittmar, M. Donegà, M. Dünser, P. Eller, C. Grab, D. Hits, W. Lustermann, B. Mangano, A.C. Marini, P. Martinez Ruiz del Arbol, D. Meister, N. Mohr, C. Nägeli³⁶, P. Nef, F. Nessi-Tedaldi, F. Pandolfi, F. Pauss, M. Peruzzi, M. Quittnat, L. Rebane, M. Rossini, A. Starodumov³⁷, M. Takahashi, K. Theofilatos, R. Wallny, H.A. Weber

Universität Zürich, Zurich, Switzerland

C. Amsler³⁸, M.F. Canelli, V. Chiochia, A. De Cosa, A. Hinzmann, T. Hreus, B. Kilminster, B. Millan Mejias, J. Ngadiuba, P. Robmann, F.J. Ronga, H. Snoek, S. Taroni, M. Verzetti, Y. Yang

National Central University, Chung-Li, Taiwan

M. Cardaci, K.H. Chen, C. Ferro, C.M. Kuo, W. Lin, Y.J. Lu, R. Volpe, S.S. Yu

National Taiwan University (NTU), Taipei, Taiwan

P. Chang, Y.H. Chang, Y.W. Chang, Y. Chao, K.F. Chen, P.H. Chen, C. Dietz, U. Grundler, W.-S. Hou, K.Y. Kao, Y.J. Lei, Y.F. Liu, R.-S. Lu, D. Majumder, E. Petrakou, Y.M. Tzeng, R. Wilken

Chulalongkorn University, Faculty of Science, Department of Physics, Bangkok, Thailand

B. Asavapibhop, N. Srimanobhas, N. Suwonjandee

Cukurova University, Adana, Turkey

A. Adiguzel, M.N. Bakirci³⁹, S. Cerci⁴⁰, C. Dozen, I. Dumanoglu, E. Eskut, S. Girgis, G. Gokbulut, E. Gurpinar, I. Hos, E.E. Kangal, A. Kayis Topaksu, G. Onengut⁴¹, K. Ozdemir, S. Ozturk³⁹, A. Polatoz, K. Sogut⁴², D. Sunar Cerci⁴⁰, B. Tali⁴⁰, H. Topakli³⁹, M. Vergili

Middle East Technical University, Physics Department, Ankara, Turkey

I.V. Akin, B. Bilin, S. Bilmis, H. Gamsizkan, G. Karapinar⁴³, K. Ocalan, U.E. Surat, M. Yalvac, M. Zeyrek

Bogazici University, Istanbul, Turkey

E. Gülmez, B. Isildak⁴⁴, M. Kaya⁴⁵, O. Kaya⁴⁵

Istanbul Technical University, Istanbul, Turkey

H. Bahtiyar⁴⁶, E. Barlas, K. Cankocak, F.I. Vardarli, M. Yücel

National Scientific Center, Kharkov Institute of Physics and Technology, Kharkov, Ukraine

L. Levchuk, P. Sorokin

University of Bristol, Bristol, United Kingdom

J.J. Brooke, E. Clement, D. Cussans, H. Flacher, R. Frazier, J. Goldstein, M. Grimes, G.P. Heath, H.F. Heath, J. Jacob, L. Kreczko, C. Lucas, Z. Meng, D.M. Newbold⁴⁷, S. Paramesvaran, A. Poll, S. Senkin, V.J. Smith, T. Williams

Rutherford Appleton Laboratory, Didcot, United Kingdom

K.W. Bell, A. Belyaev⁴⁸, C. Brew, R.M. Brown, D.J.A. Cockerill, J.A. Coughlan, K. Harder, S. Harper, E. Olaiya, D. Petyt, C.H. Shepherd-Themistocleous, A. Thea, I.R. Tomalin, W.J. Womersley, S.D. Worm

Imperial College, London, United Kingdom

M. Baber, R. Bainbridge, O. Buchmuller, D. Burton, D. Colling, N. Cripps, M. Cutajar, P. Dauncey, G. Davies, M. Della Negra, P. Dunne, W. Ferguson, J. Fulcher, D. Futyan, A. Gilbert, G. Hall, G. Iles, M. Jarvis, G. Karapostoli, M. Kenzie, R. Lane, R. Lucas⁴⁷, L. Lyons, A.-M. Magnan, S. Malik, B. Mathias, J. Nash, A. Nikitenko³⁷, J. Pela, M. Pesaresi, K. Petridis,

D.M. Raymond, S. Rogerson, A. Rose, C. Seez, P. Sharp[†], A. Tapper, M. Vazquez Acosta, T. Virdee

Brunel University, Uxbridge, United Kingdom

J.E. Cole, P.R. Hobson, A. Khan, P. Kyberd, D. Leggat, D. Leslie, W. Martin, I.D. Reid, P. Symonds, L. Teodorescu, M. Turner

Baylor University, Waco, USA

J. Dittmann, K. Hatakeyama, A. Kasmi, H. Liu, T. Scarborough

The University of Alabama, Tuscaloosa, USA

O. Charaf, S.I. Cooper, C. Henderson, P. Rumerio

Boston University, Boston, USA

A. Avetisyan, T. Bose, C. Fantasia, A. Heister, P. Lawson, C. Richardson, J. Rohlf, D. Sperka, J. St. John, L. Sulak

Brown University, Providence, USA

J. Alimena, S. Bhattacharya, G. Christopher, D. Cutts, Z. Demiragli, A. Ferapontov, A. Garabedian, U. Heintz, S. Jabeen, G. Kukartsev, E. Laird, G. Landsberg, M. Luk, M. Narain, M. Segala, T. Sinthuprasith, T. Speer, J. Swanson

University of California, Davis, Davis, USA

R. Breedon, G. Breto, M. Calderon De La Barca Sanchez, S. Chauhan, M. Chertok, J. Conway, R. Conway, P.T. Cox, R. Erbacher, M. Gardner, W. Ko, R. Lander, T. Miceli, M. Mulhearn, D. Pellett, J. Pilot, F. Ricci-Tam, M. Searle, S. Shalhout, J. Smith, M. Squires, D. Stolp, M. Tripathi, S. Wilbur, R. Yohay

University of California, Los Angeles, USA

R. Cousins, P. Everaerts, C. Farrell, J. Hauser, M. Ignatenko, G. Rakness, E. Takasugi, V. Valuev, M. Weber

University of California, Riverside, Riverside, USA

J. Babb, R. Clare, J. Ellison, J.W. Gary, G. Hanson, J. Heilman, M. Ivova Rikova, P. Jandir, E. Kennedy, F. Lacroix, H. Liu, O.R. Long, A. Luthra, M. Malberti, H. Nguyen, A. Shrinivas, S. Sumowidagdo, S. Wimpenny

University of California, San Diego, La Jolla, USA

W. Andrews, J.G. Branson, G.B. Cerati, S. Cittolin, R.T. D'Agnolo, D. Evans, A. Holzner, R. Kelley, D. Klein, M. Lebourgeois, J. Letts, I. Macneill, D. Olivito, S. Padhi, C. Palmer, M. Pieri, M. Sani, V. Sharma, S. Simon, E. Sudano, M. Tadel, Y. Tu, A. Vartak, C. Welke, F. Würthwein, A. Yagil, J. Yoo

University of California, Santa Barbara, Santa Barbara, USA

D. Barge, J. Bradmiller-Feld, C. Campagnari, T. Danielson, A. Dishaw, K. Flowers, M. Franco Sevilla, P. Geffert, C. George, F. Golf, L. Gouskos, J. Incandela, C. Justus, N. Mccoll, J. Richman, D. Stuart, W. To, C. West

California Institute of Technology, Pasadena, USA

A. Apresyan, A. Bornheim, J. Bunn, Y. Chen, E. Di Marco, J. Duarte, A. Mott, H.B. Newman, C. Pena, C. Rogan, M. Spiropulu, V. Timciuc, R. Wilkinson, S. Xie, R.Y. Zhu

Carnegie Mellon University, Pittsburgh, USA

V. Azzolini, A. Calamba, T. Ferguson, Y. Iiyama, M. Paulini, J. Russ, H. Vogel, I. Vorobiev

University of Colorado at Boulder, Boulder, USA

J.P. Cumalat, B.R. Drell, W.T. Ford, A. Gaz, E. Luiggi Lopez, U. Nauenberg, J.G. Smith, K. Stenson, K.A. Ulmer, S.R. Wagner

Cornell University, Ithaca, USA

J. Alexander, A. Chatterjee, J. Chu, S. Dittmer, N. Eggert, N. Mirman, G. Nicolas Kaufman, J.R. Patterson, A. Ryd, E. Salvati, L. Skinnari, W. Sun, W.D. Teo, J. Thom, J. Thompson, J. Tucker, Y. Weng, L. Winstrom, P. Wittich

Fairfield University, Fairfield, USA

D. Winn

Fermi National Accelerator Laboratory, Batavia, USA

S. Abdullin, M. Albrow, J. Anderson, G. Apollinari, L.A.T. Bauerdick, A. Beretvas, J. Berryhill, P.C. Bhat, K. Burkett, J.N. Butler, H.W.K. Cheung, F. Chlebana, S. Cihangir, V.D. Elvira, I. Fisk, J. Freeman, Y. Gao, E. Gottschalk, L. Gray, D. Green, S. Grünendahl, O. Gutsche, J. Hanlon, D. Hare, R.M. Harris, J. Hirschauer, B. Hooberman, S. Jindariani, M. Johnson, U. Joshi, K. Kaadze, B. Klima, B. Kreis, S. Kwan, J. Linacre, D. Lincoln, R. Lipton, T. Liu, J. Lykken, K. Maeshima, J.M. Marraffino, V.I. Martinez Outschoorn, S. Maruyama, D. Mason, P. McBride, K. Mishra, S. Mrenna, Y. Musienko³⁰, S. Nahn, C. Newman-Holmes, V. O'Dell, O. Prokofyev, E. Sexton-Kennedy, S. Sharma, A. Soha, W.J. Spalding, L. Spiegel, L. Taylor, S. Tkaczyk, N.V. Tran, L. Uplegger, E.W. Vaandering, R. Vidal, A. Whitbeck, J. Whitmore, F. Yang

University of Florida, Gainesville, USA

D. Acosta, P. Avery, D. Bourilkov, M. Carver, T. Cheng, D. Curry, S. Das, M. De Gruttola, G.P. Di Giovanni, R.D. Field, M. Fisher, I.K. Furic, J. Hugon, J. Konigsberg, A. Korytov, T. Kypreos, J.F. Low, K. Matchev, P. Milenovic⁴⁹, G. Mitselmakher, L. Muniz, A. Rinkevicius, L. Shchutska, N. Skhirtladze, M. Snowball, J. Yelton, M. Zakaria

Florida International University, Miami, USA

S. Hewamanage, S. Linn, P. Markowitz, G. Martinez, J.L. Rodriguez

Florida State University, Tallahassee, USA

T. Adams, A. Askew, J. Bochenek, B. Diamond, J. Haas, S. Hagopian, V. Hagopian, K.F. Johnson, H. Prosper, V. Veeraraghavan, M. Weinberg

Florida Institute of Technology, Melbourne, USA

M.M. Baarmand, M. Hohlmann, H. Kalakhety, F. Yumiceva

University of Illinois at Chicago (UIC), Chicago, USA

M.R. Adams, L. Apanasevich, V.E. Bazterra, D. Berry, R.R. Betts, I. Bucinskaite, R. Cavanaugh, O. Evdokimov, L. Gauthier, C.E. Gerber, D.J. Hofman, S. Khalatyan, P. Kurt, D.H. Moon, C. O'Brien, C. Silkworth, P. Turner, N. Varelas

The University of Iowa, Iowa City, USA

E.A. Albayrak⁴⁶, B. Bilki⁵⁰, W. Clarida, K. Dilsiz, F. Duru, M. Haytmyradov, J.-P. Merlo, H. Mermerkaya⁵¹, A. Mestvirishvili, A. Moeller, J. Nachtman, H. Ogul, Y. Onel, F. Ozok⁴⁶, A. Penzo, R. Rahmat, S. Sen, P. Tan, E. Tiras, J. Wetzel, T. Yetkin⁵², K. Yi

Johns Hopkins University, Baltimore, USA

B.A. Barnett, B. Blumenfeld, S. Bolognesi, D. Fehling, A.V. Gritsan, P. Maksimovic, C. Martin, M. Swartz

The University of Kansas, Lawrence, USA

P. Baringer, A. Bean, G. Benelli, C. Bruner, J. Gray, R.P. Kenny III, M. Murray, D. Noonan, S. Sanders, J. Sekaric, R. Stringer, Q. Wang, J.S. Wood

Kansas State University, Manhattan, USA

A.F. Barfuss, I. Chakaberia, A. Ivanov, S. Khalil, M. Makouski, Y. Maravin, L.K. Saini, S. Shrestha, I. Svintradze

Lawrence Livermore National Laboratory, Livermore, USA

J. Gronberg, D. Lange, F. Rebassoo, D. Wright

University of Maryland, College Park, USA

A. Baden, A. Belloni, B. Calvert, S.C. Eno, J.A. Gomez, N.J. Hadley, R.G. Kellogg, T. Kolberg, Y. Lu, M. Marionneau, A.C. Mignerey, K. Pedro, A. Skuja, M.B. Tonjes, S.C. Tonwar

Massachusetts Institute of Technology, Cambridge, USA

A. Apyan, R. Barbieri, G. Bauer, W. Busza, I.A. Cali, M. Chan, L. Di Matteo, V. Dutta, G. Gomez Ceballos, M. Goncharov, D. Gulhan, M. Klute, Y.S. Lai, Y.-J. Lee, A. Levin, P.D. Luckey, T. Ma, C. Paus, D. Ralph, C. Roland, G. Roland, G.S.F. Stephans, F. Stöckli, K. Sumorok, D. Velicanu, J. Veverka, B. Wyslouch, M. Yang, M. Zanetti, V. Zhukova

University of Minnesota, Minneapolis, USA

B. Dahmes, A. Gude, S.C. Kao, K. Klapoetke, Y. Kubota, J. Mans, N. Pastika, R. Rusack, A. Singovsky, N. Tambe, J. Turkewitz

University of Mississippi, Oxford, USA

J.G. Acosta, S. Oliveros

University of Nebraska-Lincoln, Lincoln, USA

E. Avdeeva, K. Bloom, S. Bose, D.R. Claes, A. Dominguez, R. Gonzalez Suarez, J. Keller, D. Knowlton, I. Kravchenko, J. Lazo-Flores, S. Malik, F. Meier, G.R. Snow

State University of New York at Buffalo, Buffalo, USA

J. Dolen, A. Godshalk, I. Iashvili, A. Kharchilava, A. Kumar, S. Rappoccio

Northeastern University, Boston, USA

G. Alverson, E. Barberis, D. Baumgartel, M. Chasco, J. Haley, A. Massironi, D.M. Morse, D. Nash, T. Orimoto, D. Trocino, R.J. Wang, D. Wood, J. Zhang

Northwestern University, Evanston, USA

K.A. Hahn, A. Kubik, N. Mucia, N. Odell, B. Pollack, A. Pozdnyakov, M. Schmitt, S. Stoynev, K. Sung, M. Velasco, S. Won

University of Notre Dame, Notre Dame, USA

A. Brinkerhoff, K.M. Chan, A. Drozdetskiy, M. Hildreth, C. Jessop, D.J. Karmgard, N. Kellams, K. Lannon, W. Luo, S. Lynch, N. Marinelli, T. Pearson, M. Planer, R. Ruchti, N. Valls, M. Wayne, M. Wolf, A. Woodard

The Ohio State University, Columbus, USA

L. Antonelli, J. Brinson, B. Bylsma, L.S. Durkin, S. Flowers, C. Hill, R. Hughes, K. Kotov, T.Y. Ling, D. Puigh, M. Rodenburg, G. Smith, C. Vuosalo, B.L. Winer, H. Wolfe, H.W. Wulsin

Princeton University, Princeton, USA

E. Berry, O. Driga, P. Elmer, P. Hebda, A. Hunt, S.A. Koay, P. Lujan, D. Marlow, T. Medvedeva, M. Mooney, J. Olsen, P. Piroué, X. Quan, H. Saka, D. Stickland², C. Tully, J.S. Werner, S.C. Zenz, A. Zuranski

University of Puerto Rico, Mayaguez, USA

E. Brownson, H. Mendez, J.E. Ramirez Vargas

Purdue University, West Lafayette, USA

E. Alagoz, V.E. Barnes, D. Benedetti, G. Bolla, D. Bortoletto, M. De Mattia, Z. Hu, M.K. Jha, M. Jones, K. Jung, M. Kress, N. Leonardo, D. Lopes Pegna, V. Maroussov, P. Merkel, D.H. Miller, N. Neumeister, B.C. Radburn-Smith, X. Shi, I. Shipsey, D. Silvers, A. Svyatkovskiy, F. Wang, W. Xie, L. Xu, H.D. Yoo, J. Zablocki, Y. Zheng

Purdue University Calumet, Hammond, USA

N. Parashar, J. Stupak

Rice University, Houston, USA

A. Adair, B. Akgun, K.M. Ecklund, F.J.M. Geurts, W. Li, B. Michlin, B.P. Padley, R. Redjimi, J. Roberts, J. Zabel

University of Rochester, Rochester, USA

B. Betchart, A. Bodek, R. Covarelli, P. de Barbaro, R. Demina, Y. Eshaq, T. Ferbel, A. Garcia-Bellido, P. Goldenzweig, J. Han, A. Harel, A. Khukhunaishvili, D.C. Miner, G. Petrillo, D. Vishnevskiy

The Rockefeller University, New York, USA

R. Ciesielski, L. Demortier, K. Goulianos, G. Lungu, C. Mesropian

Rutgers, The State University of New Jersey, Piscataway, USA

S. Arora, A. Barker, J.P. Chou, C. Contreras-Campana, E. Contreras-Campana, D. Duggan, D. Ferencek, Y. Gershtein, R. Gray, E. Halkiadakis, D. Hidas, A. Lath, S. Panwalkar, M. Park, R. Patel, V. Rekovic, S. Salur, S. Schnetzer, C. Seitz, S. Somalwar, R. Stone, S. Thomas, P. Thomassen, M. Walker

University of Tennessee, Knoxville, USA

K. Rose, S. Spanier, A. York

Texas A&M University, College Station, USA

O. Bouhali⁵³, R. Eusebi, W. Flanagan, J. Gilmore, T. Kamon⁵⁴, V. Khotilovich, V. Krutelyov, R. Montalvo, I. Osipenkov, Y. Pakhotin, A. Perloff, J. Roe, A. Rose, A. Safonov, T. Sakuma, I. Suarez, A. Tatarinov

Texas Tech University, Lubbock, USA

N. Akchurin, C. Cowden, J. Damgov, C. Dragoiu, P.R. Duderu, J. Faulkner, K. Kovitanggoon, S. Kunori, S.W. Lee, T. Libeiro, I. Volobouev

Vanderbilt University, Nashville, USA

E. Appelt, A.G. Delannoy, S. Greene, A. Gurrola, W. Johns, C. Maguire, Y. Mao, A. Melo, M. Sharma, P. Sheldon, B. Snook, S. Tuo, J. Velkovska

University of Virginia, Charlottesville, USA

M.W. Arenton, S. Boutle, B. Cox, B. Francis, J. Goodell, R. Hirosky, A. Ledovskoy, H. Li, C. Lin, C. Neu, J. Wood

Wayne State University, Detroit, USA

S. Gollapinni, R. Harr, P.E. Karchin, C. Kottachchi Kankanamge Don, P. Lamichhane, J. Sturdy

University of Wisconsin, Madison, USA

D.A. Belknap, D. Carlsmith, M. Cepeda, S. Dasu, S. Duric, E. Friis, R. Hall-Wilton, M. Herndon,

A. Hervé, P. Klabbers, A. Lanaro, C. Lazaridis, A. Levine, R. Loveless, A. Mohapatra, I. Ojalvo, T. Perry, G.A. Pierro, G. Polese, I. Ross, T. Sarangi, A. Savin, W.H. Smith, N. Woods

†: Deceased

- 1: Also at Vienna University of Technology, Vienna, Austria
- 2: Also at CERN, European Organization for Nuclear Research, Geneva, Switzerland
- 3: Also at Institut Pluridisciplinaire Hubert Curien, Université de Strasbourg, Université de Haute Alsace Mulhouse, CNRS/IN2P3, Strasbourg, France
- 4: Also at National Institute of Chemical Physics and Biophysics, Tallinn, Estonia
- 5: Also at Skobeltsyn Institute of Nuclear Physics, Lomonosov Moscow State University, Moscow, Russia
- 6: Also at Universidade Estadual de Campinas, Campinas, Brazil
- 7: Also at California Institute of Technology, Pasadena, USA
- 8: Also at Laboratoire Leprince-Ringuet, Ecole Polytechnique, IN2P3-CNRS, Palaiseau, France
- 9: Also at Joint Institute for Nuclear Research, Dubna, Russia
- 10: Also at Suez University, Suez, Egypt
- 11: Also at British University in Egypt, Cairo, Egypt
- 12: Also at Fayoum University, El-Fayoum, Egypt
- 13: Now at Ain Shams University, Cairo, Egypt
- 14: Also at Université de Haute Alsace, Mulhouse, France
- 15: Also at Brandenburg University of Technology, Cottbus, Germany
- 16: Also at The University of Kansas, Lawrence, USA
- 17: Also at Institute of Nuclear Research ATOMKI, Debrecen, Hungary
- 18: Also at Eötvös Loránd University, Budapest, Hungary
- 19: Also at University of Debrecen, Debrecen, Hungary
- 20: Now at King Abdulaziz University, Jeddah, Saudi Arabia
- 21: Also at University of Visva-Bharati, Santiniketan, India
- 22: Also at University of Ruhuna, Matara, Sri Lanka
- 23: Also at Isfahan University of Technology, Isfahan, Iran
- 24: Also at Sharif University of Technology, Tehran, Iran
- 25: Also at Plasma Physics Research Center, Science and Research Branch, Islamic Azad University, Tehran, Iran
- 26: Also at Università degli Studi di Siena, Siena, Italy
- 27: Also at Centre National de la Recherche Scientifique (CNRS) - IN2P3, Paris, France
- 28: Also at Purdue University, West Lafayette, USA
- 29: Also at Universidad Michoacana de San Nicolas de Hidalgo, Morelia, Mexico
- 30: Also at Institute for Nuclear Research, Moscow, Russia
- 31: Also at St. Petersburg State Polytechnical University, St. Petersburg, Russia
- 32: Also at Faculty of Physics, University of Belgrade, Belgrade, Serbia
- 33: Also at Facoltà Ingegneria, Università di Roma, Roma, Italy
- 34: Also at Scuola Normale e Sezione dell'INFN, Pisa, Italy
- 35: Also at University of Athens, Athens, Greece
- 36: Also at Paul Scherrer Institut, Villigen, Switzerland
- 37: Also at Institute for Theoretical and Experimental Physics, Moscow, Russia
- 38: Also at Albert Einstein Center for Fundamental Physics, Bern, Switzerland
- 39: Also at Gaziosmanpasa University, Tokat, Turkey
- 40: Also at Adiyaman University, Adiyaman, Turkey
- 41: Also at Cag University, Mersin, Turkey
- 42: Also at Mersin University, Mersin, Turkey
- 43: Also at Izmir Institute of Technology, Izmir, Turkey

44: Also at Ozyegin University, Istanbul, Turkey

45: Also at Kafkas University, Kars, Turkey

46: Also at Mimar Sinan University, Istanbul, Istanbul, Turkey

47: Also at Rutherford Appleton Laboratory, Didcot, United Kingdom

48: Also at School of Physics and Astronomy, University of Southampton, Southampton, United Kingdom

49: Also at University of Belgrade, Faculty of Physics and Vinca Institute of Nuclear Sciences, Belgrade, Serbia

50: Also at Argonne National Laboratory, Argonne, USA

51: Also at Erzincan University, Erzincan, Turkey

52: Also at Yildiz Technical University, Istanbul, Turkey

53: Also at Texas A&M University at Qatar, Doha, Qatar

54: Also at Kyungpook National University, Daegu, Korea